

~~CONFIDENTIAL~~

6

RM A511.03

NACARM A511.03

FEB 20 1952

CLASSIFICATION CHANGED

~~CONFIDENTIAL~~~~RECORDED~~~~SECURITY INFORMATION~~

To:

SECURITY INFORMATION

NACA

X. L. Dryden per race plane  
By authority of Farm 1391-4/10/3 Date Feb 5/15/3

## RESEARCH MEMORANDUM

TESTS IN THE AMES 40- BY 80-FOOT WIND TUNNEL OF AN AIRPLANE

CONFIGURATION WITH AN ASPECT RATIO 2 TRIANGULAR WING

AND AN ALL-MOVABLE HORIZONTAL TAIL -

LATERAL CHARACTERISTICS

By David Graham and David G. Koenig

Ames Aeronautical Laboratory  
Moffett Field, Calif.

CLASSIFICATION CHANGED

CLASSIFICATION CANCELLED

Authority NACA Ref. 6-6 Date 12/14/55  
R.N. No. 94  
By 2nd Lt. 1/16/56 See

To:

*Confidential*

Date 12/1/53

This material contains information affecting the National Defense of the United States within the meaning of the espionage laws, Title 18, U.S.C., Secs. 793 and 794, the transmission or revelation of which in any manner to unauthorized person is prohibited by law.

NATIONAL ADVISORY COMMITTEE  
FOR AERONAUTICS

WASHINGTON

February 11, 1952

~~CONFIDENTIAL~~~~SECURITY INFORMATION~~

CONFIDENTIAL NACA LIBRARY

LANGLEY AERONAUTICAL LABORATORY  
Langley Field, Va.

~~CONFIDENTIAL~~

SECURITY INFORMATION

NATIONAL ADVISORY COMMITTEE FOR AERONAUTICS

RESEARCH MEMORANDUM

TESTS IN THE AMES 40- BY 80-FOOT WIND TUNNEL OF AN AIRPLANE  
CONFIGURATION WITH AN ASPECT RATIO 2 TRIANGULAR WING  
AND AN ALL-MOVABLE HORIZONTAL TAIL -

## LATERAL CHARACTERISTICS

By David Graham and David G. Koenig

## SUMMARY

An investigation has been made to determine the low-speed lateral characteristics of a triangular-wing airplane model. The model consisted of an aspect ratio 2 triangular wing in combination with a fuselage of fineness ratio 12.5; a thin, triangular, vertical tail with a constant-chord rudder; and a thin, unswept, all-movable horizontal tail. The wing had an NACA 0005 modified section and was equipped with partial-span, slotted, trailing-edge flaps. Tests were made with the wing alone, wing-fuselage, and wing-fuselage-vertical-tail configurations in addition to the tests of the complete model. The Reynolds number, based on the wing mean aerodynamic chord, was approximately  $14.6 \times 10^6$  and the Mach number was 0.13.

## INTRODUCTION

A study of the low-speed characteristics of an airplane configuration with an aspect ratio 2 triangular wing and an all-movable horizontal tail has been undertaken in the Ames 40- by 80-foot wind tunnel. The results of tests to determine the longitudinal characteristics, reported in reference 1, showed that of the three vertical positions of the horizontal tail used, namely, 0-, 25-, and 50-percent wing semispan above the wing-chord plane, only the lowest provided satisfactory longitudinal stability. Accordingly, this position of the horizontal tail was selected for the investigation of the low-speed aerodynamic characteristics of the airplane configuration in sideslip. The investigation also

~~CONFIDENTIAL~~

SECURITY INFORMATION

included tests of the wing alone, wing-fuselage, and wing-fuselage-vertical-tail combinations. The results are presented herein without analysis in order to expedite publication.

#### NOTATION

The coefficients and symbols used within this report are defined as follows and in figure 1. The moment data are referred to a moment center located at 42.6 percent of the mean aerodynamic chord.

- a angle of attack of the wing-chord plane with reference to free stream, degrees
- b wing span, feet
- $b_t$  horizontal-tail span, feet
- c wing chord, measured parallel to wing center line, feet
- $\bar{c}$  mean aerodynamic chord of wing, measured parallel to wing

$$\text{center line } \left( \frac{\int_0^{b/2} c^2 dy}{\int_0^{b/2} c dy} \right), \text{ feet}$$

- $C_D$  drag coefficient  $\left( \frac{\text{drag}}{qS} \right)$
- $C_I$  rolling-moment coefficient  $\left( \frac{\text{rolling moment}}{qSb} \right)$
- $C_L$  lift coefficient  $\left( \frac{\text{lift}}{qS} \right)$
- $C_m$  pitching-moment coefficient  $\left( \frac{\text{pitching moment}}{qS\bar{c}} \right)$
- $C_n$  yawing-moment coefficient  $\left( \frac{\text{yawing moment}}{qSb} \right)$
- $C_Y$  side-force coefficient  $\left( \frac{\text{side force}}{qS} \right)$
- $\delta_a$  total aileron deflection, measured perpendicular to hinge line, degrees
- $\delta_f$  flap deflection, measured perpendicular to hinge line, degrees
- $\delta_r$  rudder deflection, measured perpendicular to hinge line, degrees

- $i_t$  horizontal-tail incidence relative to the wing-chord plane, degrees
- $l_t$  distance from moment center of model to pivot line of horizontal tail, feet
- $p$  rate of rolling, radians per second
- $\frac{pb}{2V}$  wing-tip helix angle, radians
- $q$  free-stream dynamic pressure, pounds per square foot
- $S$  wing area, square feet
- $S_t$  horizontal-tail area, square feet
- $V$  free-stream velocity, feet per second
- $\phi$  angle of bank, right bank positive, degrees
- $x$  longitudinal coordinate parallel to model center line, feet
- $y$  lateral coordinate perpendicular to plane of symmetry, feet
- $z$  vertical coordinate perpendicular to wing-chord plane, feet
- $c_{l\beta} \left( \frac{\partial c_l}{\partial \beta} \right)$
- $c_{n\beta} \left( \frac{\partial c_n}{\partial \beta} \right)$
- $c_{y\beta} \left( \frac{\partial c_y}{\partial \beta} \right)$

## APPARATUS, TESTS, AND RESULTS

A drawing of the complete airplane model is shown in figure 2, and the pertinent dimensional data are presented in table I. The model was identical in all respects, except for the addition of a rudder, to that described in reference 1. The constant-chord rudder had a plain radius nose and a small but unsealed gap.

The tests conducted are listed in table II, which also serves as an index to figures 3 through 14 where the data are presented. (It should be noted that a dashed-line fairing is used in figures 4, 8, 10, and 14 where the data are incomplete.) The horizontal-tail incidences were chosen to provide data at low trim lift coefficients and at trim lift coefficients near those suitable for landing. The asymmetric flap deflections (fig. 13) were used to give an indication of the effectiveness of the trailing-edge flaps when used as ailerons. The moment data are referred to a moment center located at 42.6 percent of the mean aerodynamic chord. This is the moment center for which a value of  $(dC_m/dC_L)_{C_L=0} = -0.06$  would be obtained when the trailing-edge flaps and

the horizontal tail are undeflected. The data were corrected for wind-tunnel-wall effects and support-strut interference. Accuracy of all control surface and flap deflections was within  $\pm 0.2^\circ$ . No corrections have been applied to the data for possible deflection due to aerodynamic loads since they were believed to be negligible.

The stability derivatives as measured at  $0^\circ$  of sideslip are presented in figure 15. The increments of  $C_l$ ,  $C_n$ , and  $C_y$  per degree of aileron deflection, as measured with  $\Delta\delta_a = 10^\circ$  superposed on  $5^\circ$  and  $35^\circ$  flap deflections, are shown in figure 16. Figure 17 shows the variation of  $p_b/2V$  with lift coefficient computed for the complete model at  $\beta = 0^\circ$  and with  $\delta_f = 5^\circ$  and  $\delta_a = 10^\circ$ . The values of damping-in-roll coefficient as given in reference 2 were used for the computation of  $p_b/2V$ . The increments of  $C_l$ ,  $C_n$ , and  $C_y$  per degree of rudder deflection, as measured with  $\Delta\delta_r = 10^\circ$ , are presented in figure 18. As a final summary, the control deflection necessary to hold steady sideslip and the resultant angle of bank for the model with the flaps deflected  $40^\circ$  are shown in figure 19 for lift coefficients of 0.4, 0.8, and 1.2. Although data were obtained only for  $10^\circ$  total aileron deflection and  $10^\circ$  rudder deflection, the curves of figure 19 were extended to  $30^\circ$  total aileron deflection and to rudder deflection greater than  $10^\circ$ , by using a linear extrapolation of the increments of  $C_l$ ,  $C_n$ , and  $C_y$  due to aileron or rudder deflection, in order to indicate possible limits of control.

The average Reynolds number of the tests was 14.6 million based on the mean aerodynamic chord of the wing. The dynamic pressure was approximately 25 pounds per square foot and the Mach number was 0.13.

Ames Aeronautical Laboratory,  
National Advisory Committee for Aeronautics,  
Moffett Field, Calif.

## REFERENCES

1. Graham, David, and Koenig, David G.: Tests in the Ames 40- by 80-Foot Wind Tunnel of an Airplane Configuration With an Aspect Ratio 2 Triangular Wing and an All-Movable Horizontal Tail - Longitudinal Characteristics. NACA RM A51B21, 1951.
2. Tosti, Louis P.: Low-Speed Static Stability and Damping-in-Roll Characteristics of Some Swept and Unswept Low-Aspect-Ratio Wings. NACA TN 1468, 1947.

TABLE I. - DIMENSIONAL DATA

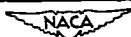
Wing	
Area, square feet . . . . .	312.5
Span, feet . . . . .	25.00
Mean aerodynamic chord, feet . . . . .	16.67
Aspect ratio . . . . .	2
Taper ratio . . . . .	0
Airfoil section parallel to wing center line . . . . .	NACA 0005 (mod)
Fuselage	
Length, feet . . . . .	56.16
Maximum diameter, feet . . . . .	4.49
Fineness ratio . . . . .	12.5
Vertical tail	
Exposed area, square feet . . . . .	52.53
Aspect ratio of plan form, extended to model center line . . . . .	1
Taper ratio . . . . .	0
Airfoil section parallel to model center line . . . . .	NACA 0005 (mod)
Rudder area (exposed), square feet . . . . .	12.87
Slotted, trailing-edge flaps	
Area (total movable), square feet . . . . .	37.44
Chord . . . . .	0.2084c
Horizontal tail	
$S_t/S$ . . . . .	0.246
$b_t/b$ . . . . .	0.738
$l_t/c$ (moment center at $0.426c$ ) . . . . .	1.161
Aspect ratio . . . . .	4.4
Taper ratio . . . . .	0.46

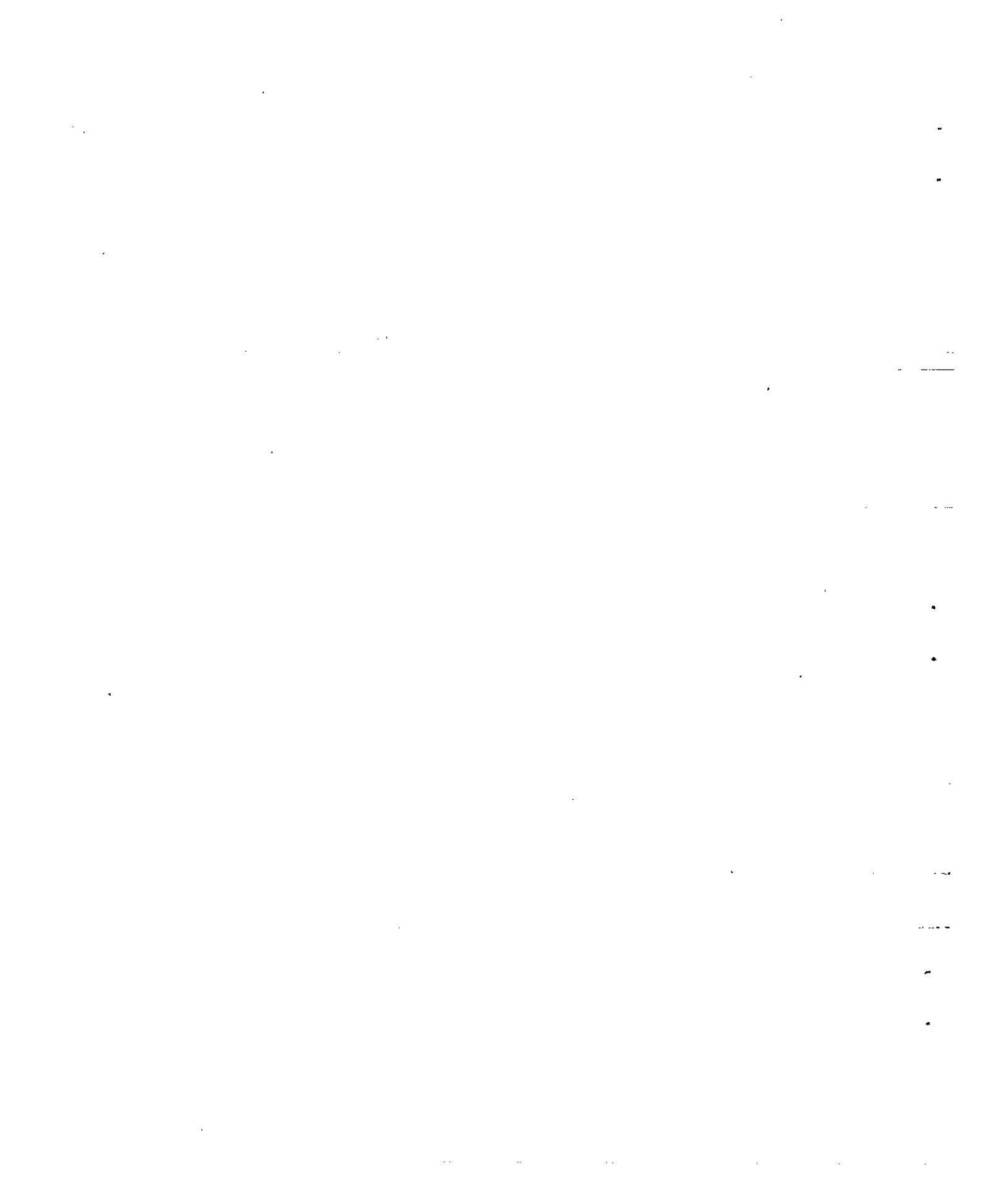
NACA

TABLE II. - SUMMARY OF CONFIGURATIONS TESTED

Figure	Configuration	Control deflection (deg)			$\beta$ (deg)	$\alpha$ (deg) (nominal)	Data
		$\delta_f$	$\delta_t$	$\delta_r$			
3(a) (b)	W alone	0	-	-	0,12	-1 → 26	$C_L$ vs $\alpha$ , $C_D$ , $C_m$
					0,12	-1 → 26	$C_L$ vs $C_l$ , $C_n$ , $C_Y$
4(a) (b)	W alone	0	-	-	0 → 12	0,8,16,20	$C_L$ , $C_D$ , $C_m$ vs $\beta$
					0 → 12	0,8,16,20	$C_l$ , $C_n$ , $C_Y$ vs $\beta$
5(a) (b)	W + F	0,40	-	-	0,12	-1 → 26	$C_L$ vs $\alpha$ , $C_D$ , $C_m$
					0,12	-1 → 26	$C_L$ vs $C_l$ , $C_n$ , $C_Y$
6(a) (b)	W + F	0,40	-	-	-2 → 12	0,8,16,20	$C_L$ , $C_D$ , $C_m$ vs $\beta$
					-2 → 12	0,8,16,20	$C_l$ , $C_n$ , $C_Y$ vs $\beta$
7(a) (b)	W + F + V	0,40	-	0	0,12	-1 → 26	$C_L$ vs $\alpha$ , $C_D$ , $C_m$
					0,12	-1 → 26	$C_L$ vs $C_l$ , $C_n$ , $C_Y$
8(a) (b)	W + F + V	0,40	-	0	0 → 12	0,8,16,20	$C_L$ , $C_D$ , $C_m$ vs $\beta$
					0 → 12	0,8,16,20	$C_l$ , $C_n$ , $C_Y$ vs $\beta$
9(a) (b)	W + F + V + H	0,40	0	0	0,12	-1 → 26	$C_L$ vs $\alpha$ , $C_D$ , $C_m$
					0,12	-1 → 26	$C_L$ vs $C_l$ , $C_n$ , $C_Y$
10(a) (b)	W + F + V + H	0,40	0	0	-2 → 12	0,8,16,20	$C_L$ , $C_D$ , $C_m$ vs $\beta$
					-2 → 12	0,8,16,20	$C_l$ , $C_n$ , $C_Y$ vs $\beta$
11(a) (b)	W + F + V + H	0,40	-10	0	0,12	-1 → 26	$C_L$ vs $\alpha$ , $C_D$ , $C_m$
					0,12	-1 → 26	$C_L$ vs $C_l$ , $C_n$ , $C_Y$
12(a) (b)	W + F + V + H	0,40	-10	0	-2 → 12	0,8,16,20	$C_L$ , $C_D$ , $C_m$ vs $\beta$
					-2 → 12	0,8,16,20	$C_l$ , $C_n$ , $C_Y$ vs $\beta$
13(a) (b)	W + F + V + H	lh,10 rh,0 lh,40 rh,30	-10	0	-2 → 12	0,8,16,20	$C_L$ , $C_D$ , $C_m$ vs $\beta$
					-2 → 12	0,8,16,20	$C_l$ , $C_n$ , $C_Y$ vs $\beta$
14	W + F + V W + F + V + H	0,40	0, -10	10	-2 → 12	0,8,16,20	$C_l$ , $C_n$ , $C_Y$ vs $\beta$

NOTE: W, wing; F, fuselage; V, vertical tail; H, horizontal tail.





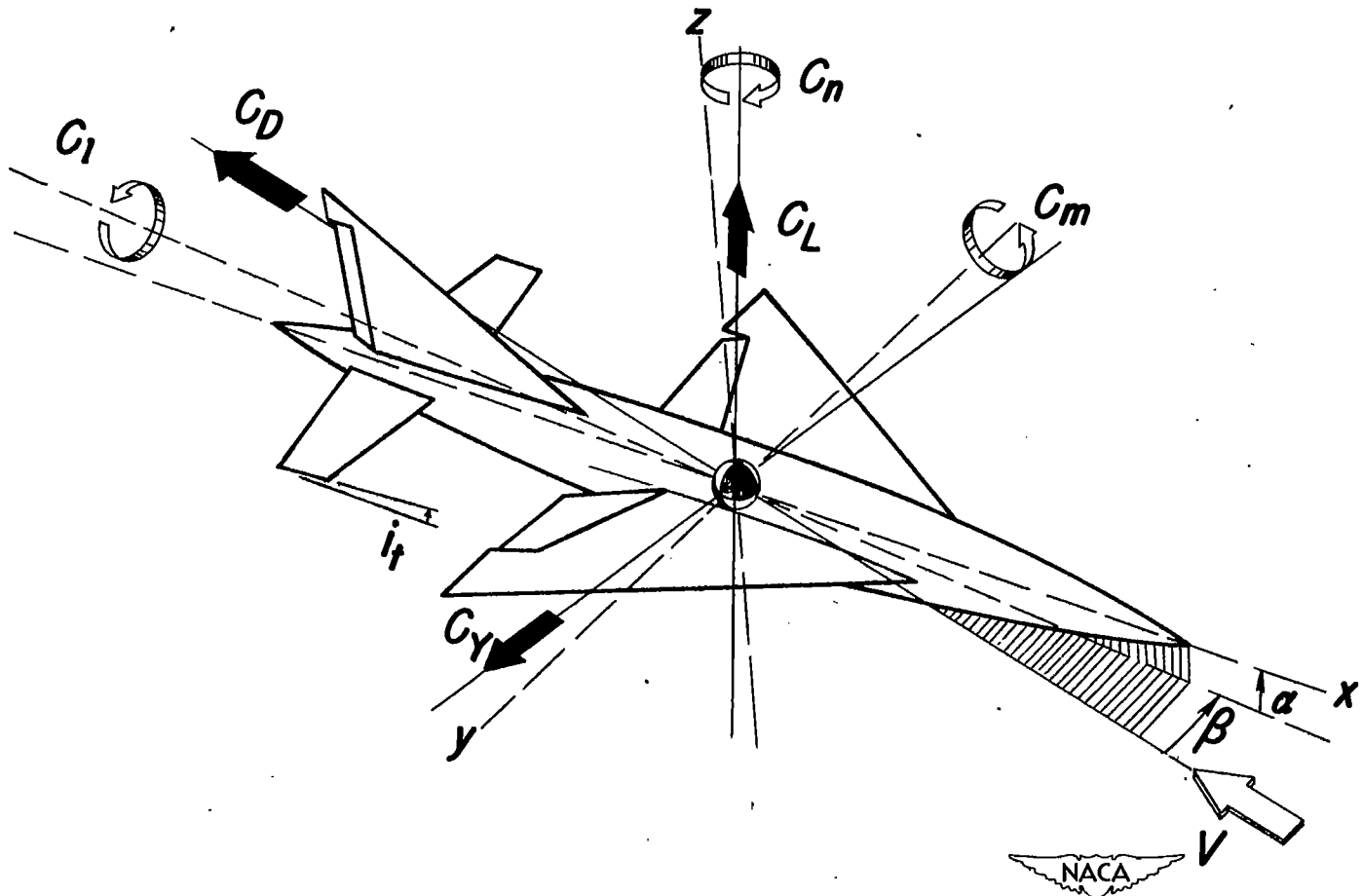


Figure 1.— Sign convention for force and moment coefficients. All force and moment coefficients, angles and control-surface deflections are shown as positive.

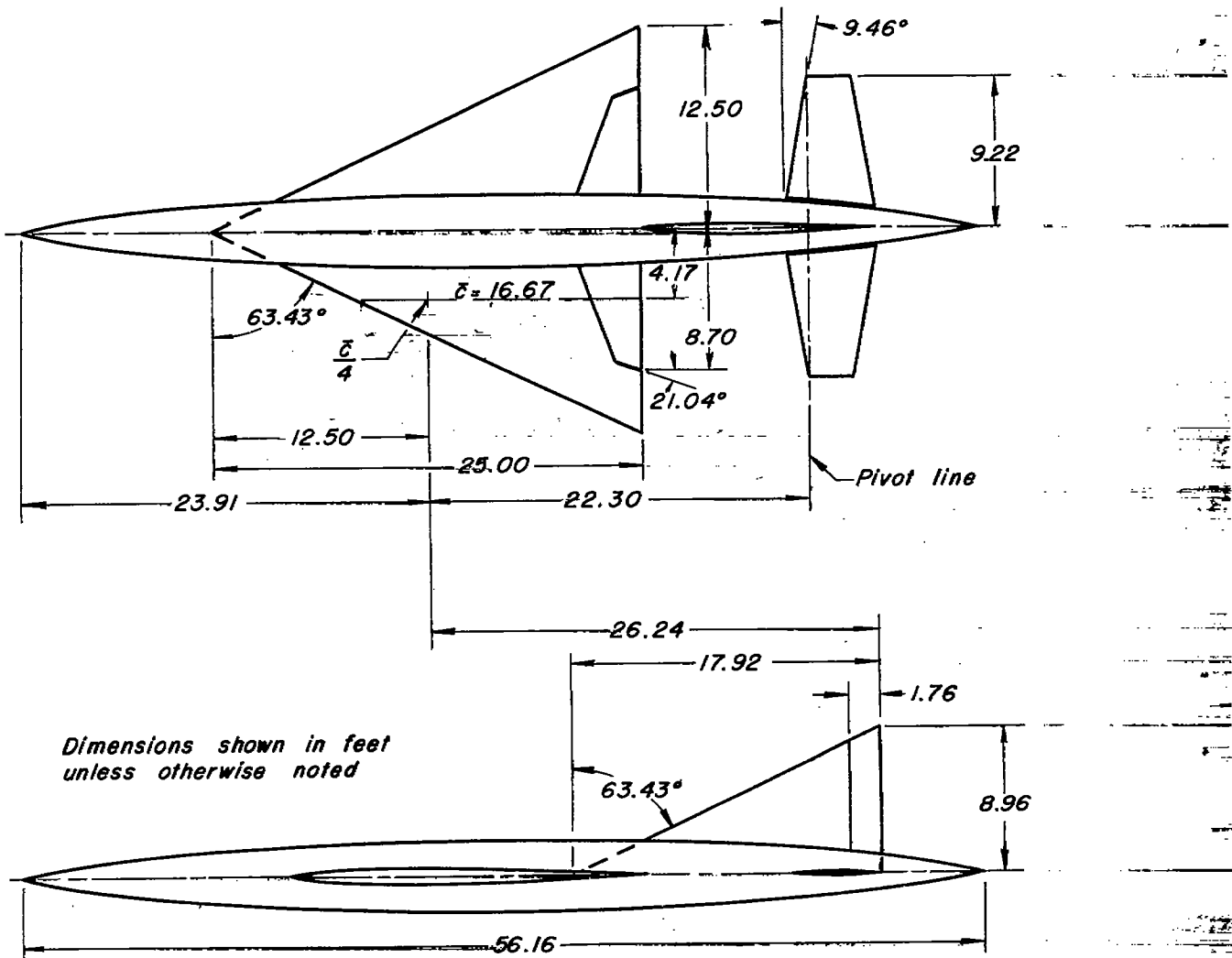


Figure 2.— Geometric details of the model.

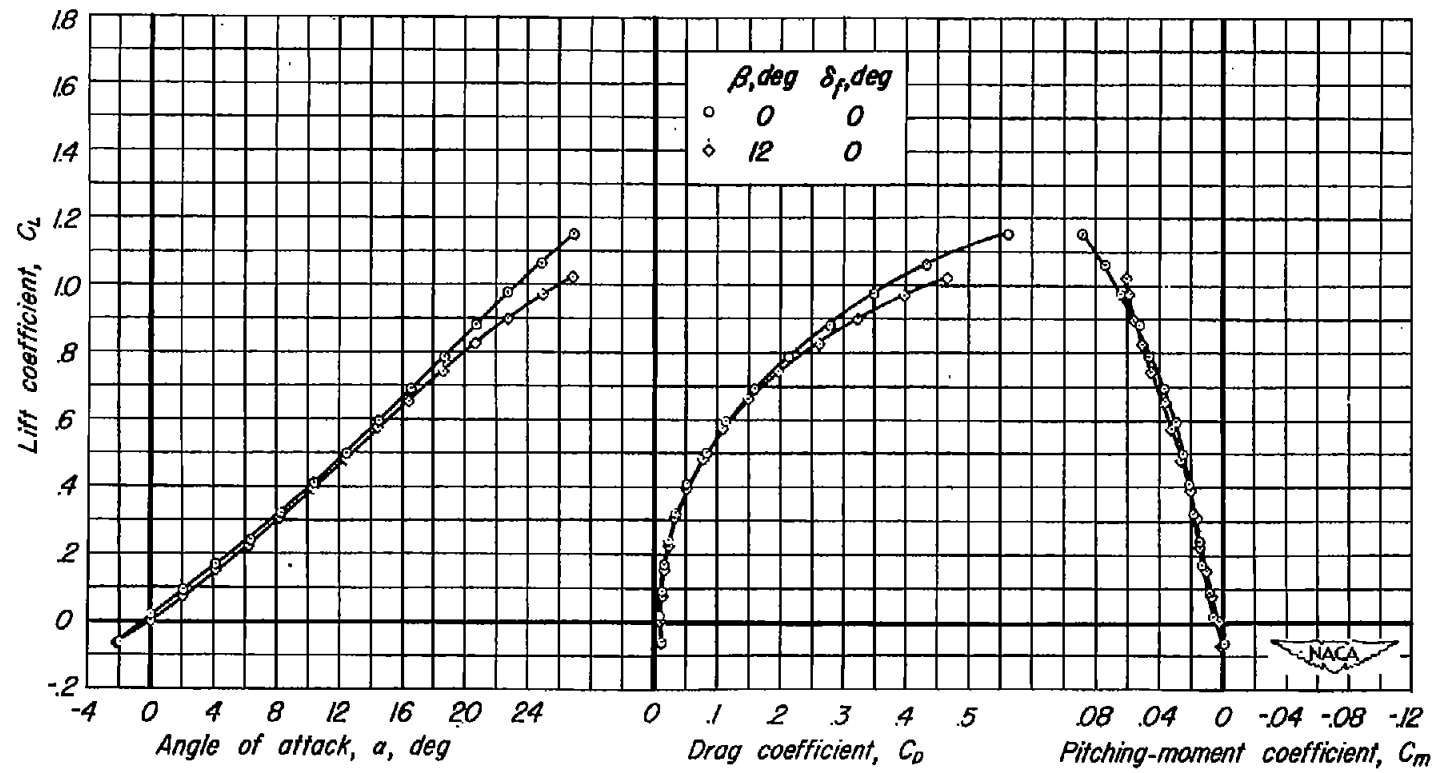
(a)  $C_L$  vs  $\alpha$ ,  $C_D$ ,  $C_m$ 

Figure 3.—Characteristics of the wing alone at two angles of sideslip.

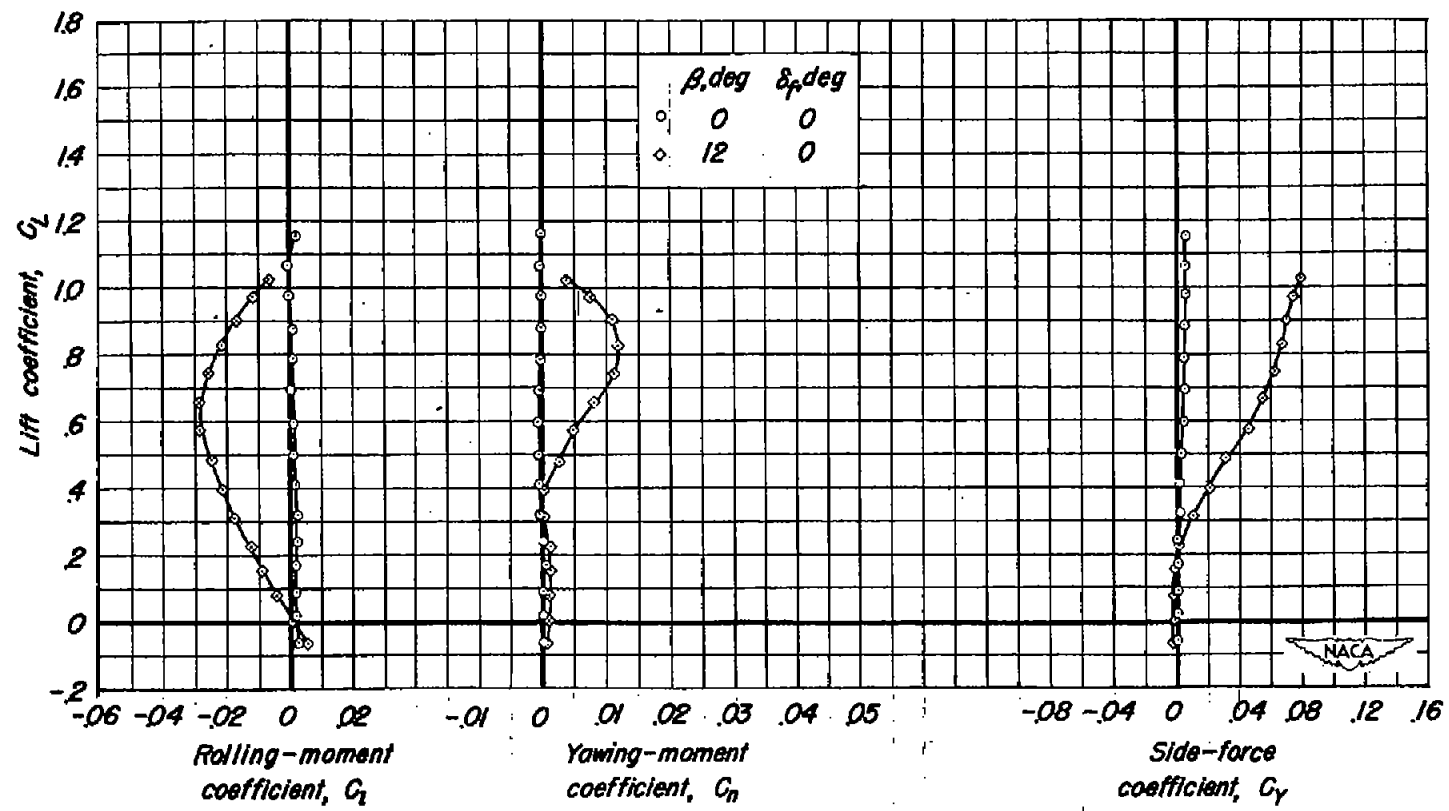
(b)  $C_L$  vs  $C_I$ ,  $C_n$ ,  $C_Y$ 

Figure 3.—Concluded.

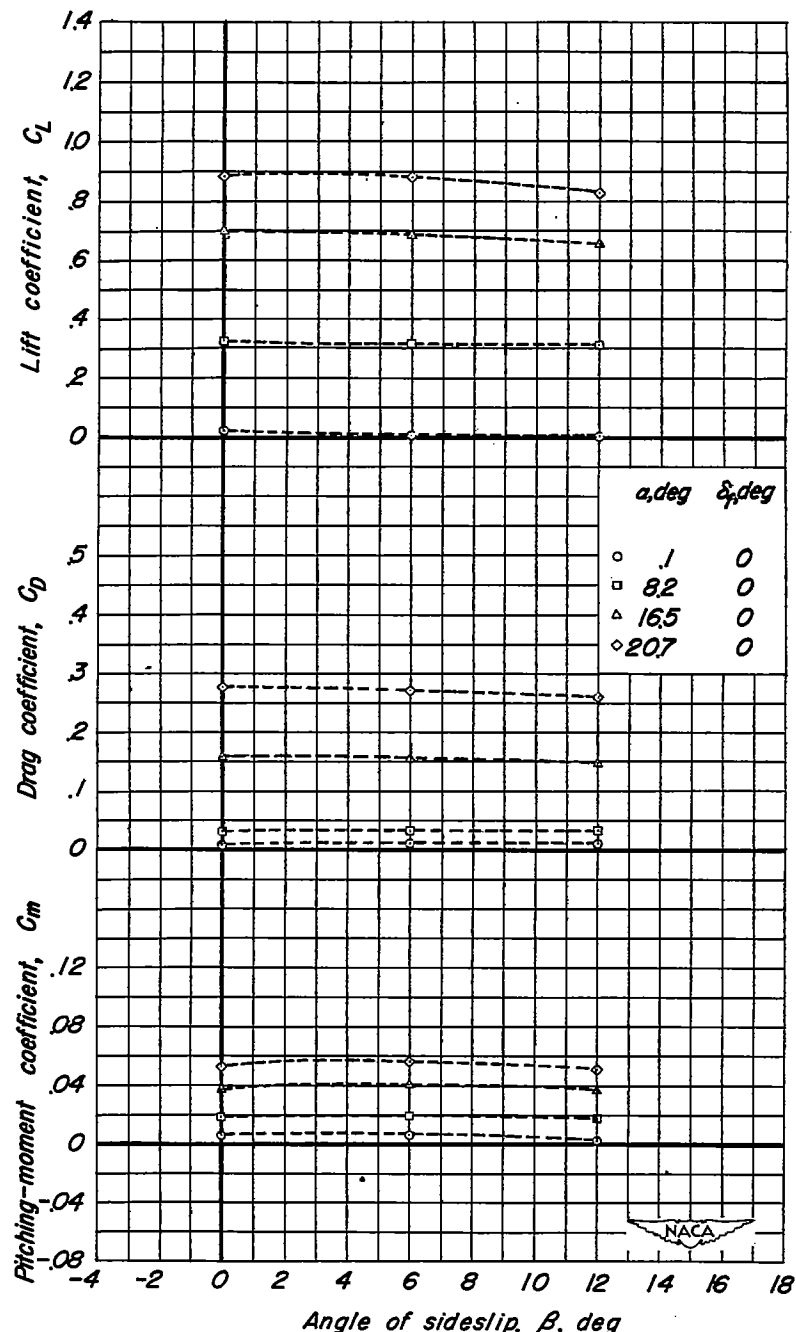
(a)  $C_L$ ,  $C_D$ ,  $C_m$  vs  $\beta$ 

Figure 4.—Characteristics in sideslip of the wing alone.

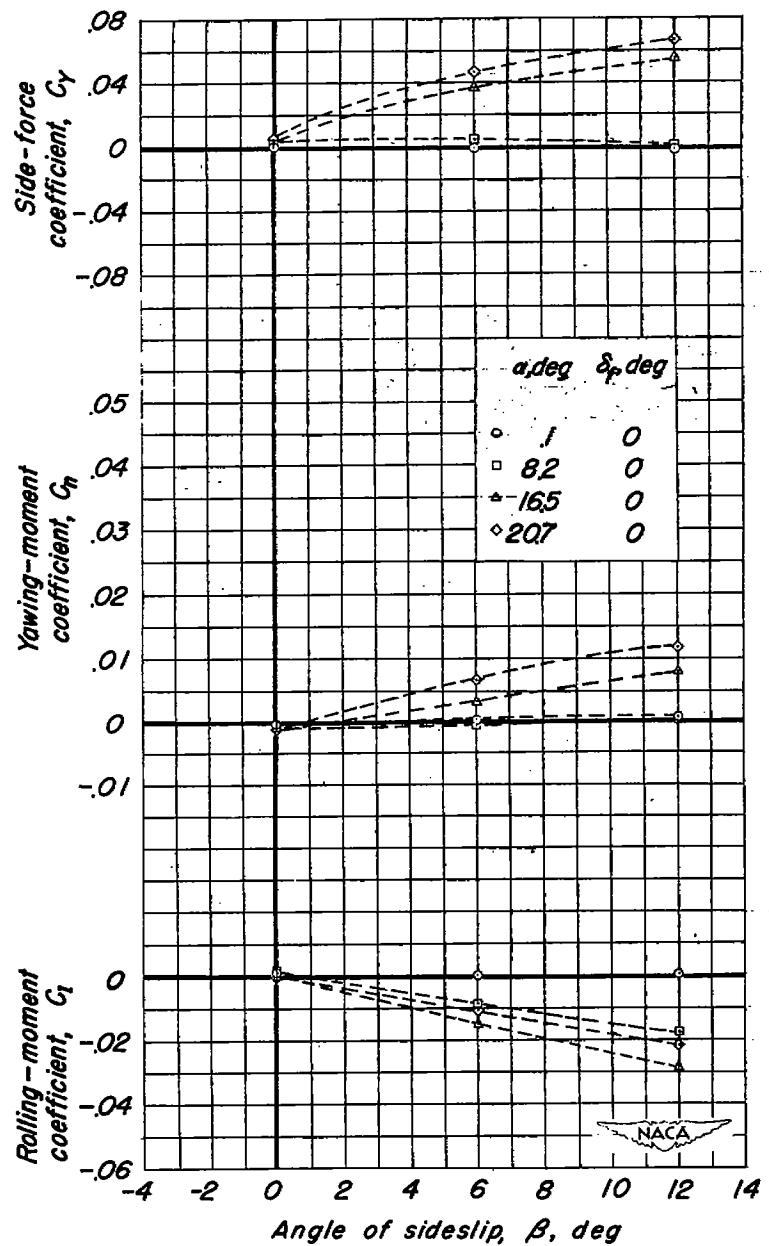
(b)  $C_y$ ,  $C_n$ ,  $C_r$  vs  $\beta$ 

Figure 4.—Concluded.

*CONFIDENTIAL*

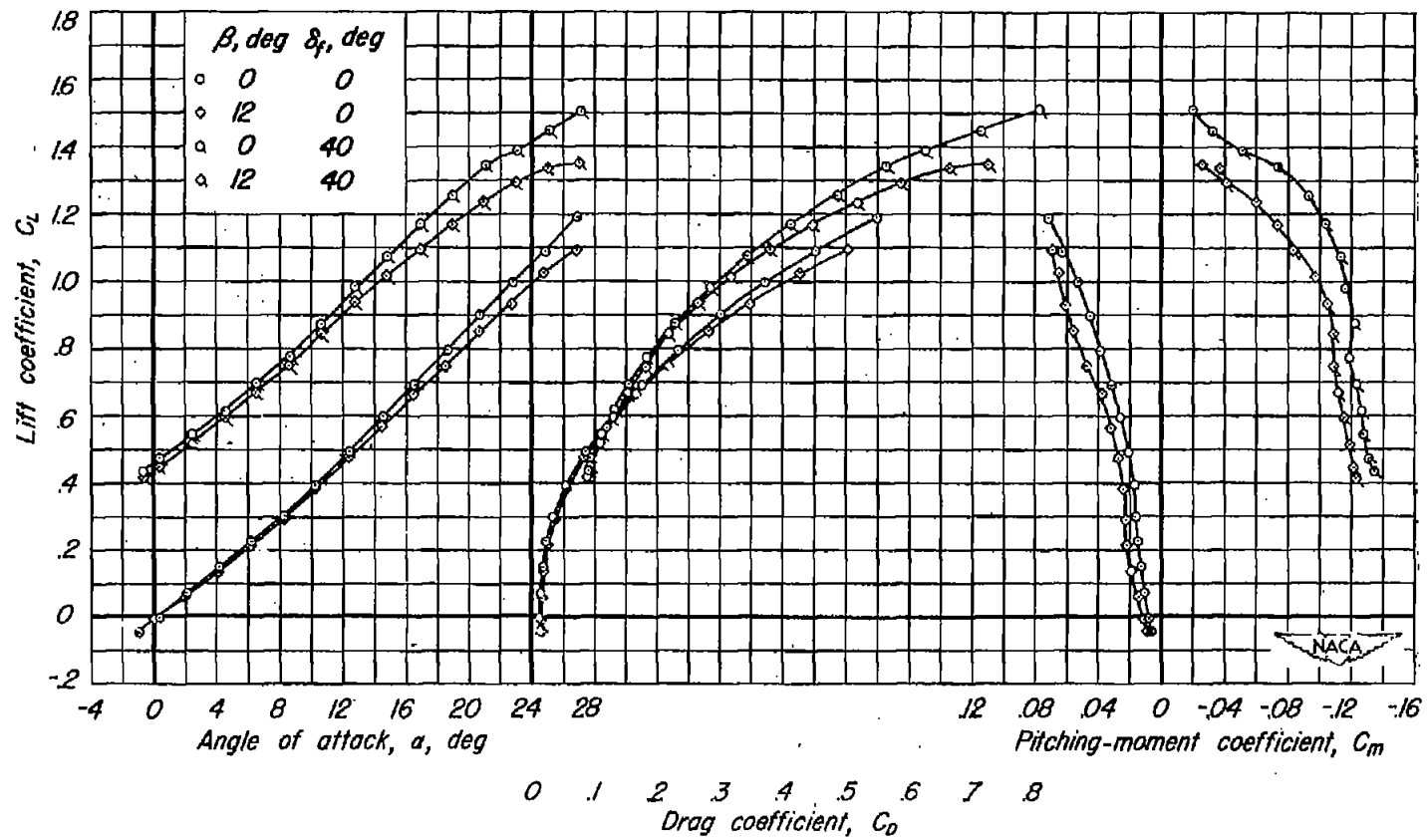
(a)  $C_L$  vs  $\alpha$ ,  $C_D$ ,  $C_m$ 

Figure 5.—Characteristics of the wing-fuselage configuration at two angles of sideslip and with two trailing-edge flap deflections.

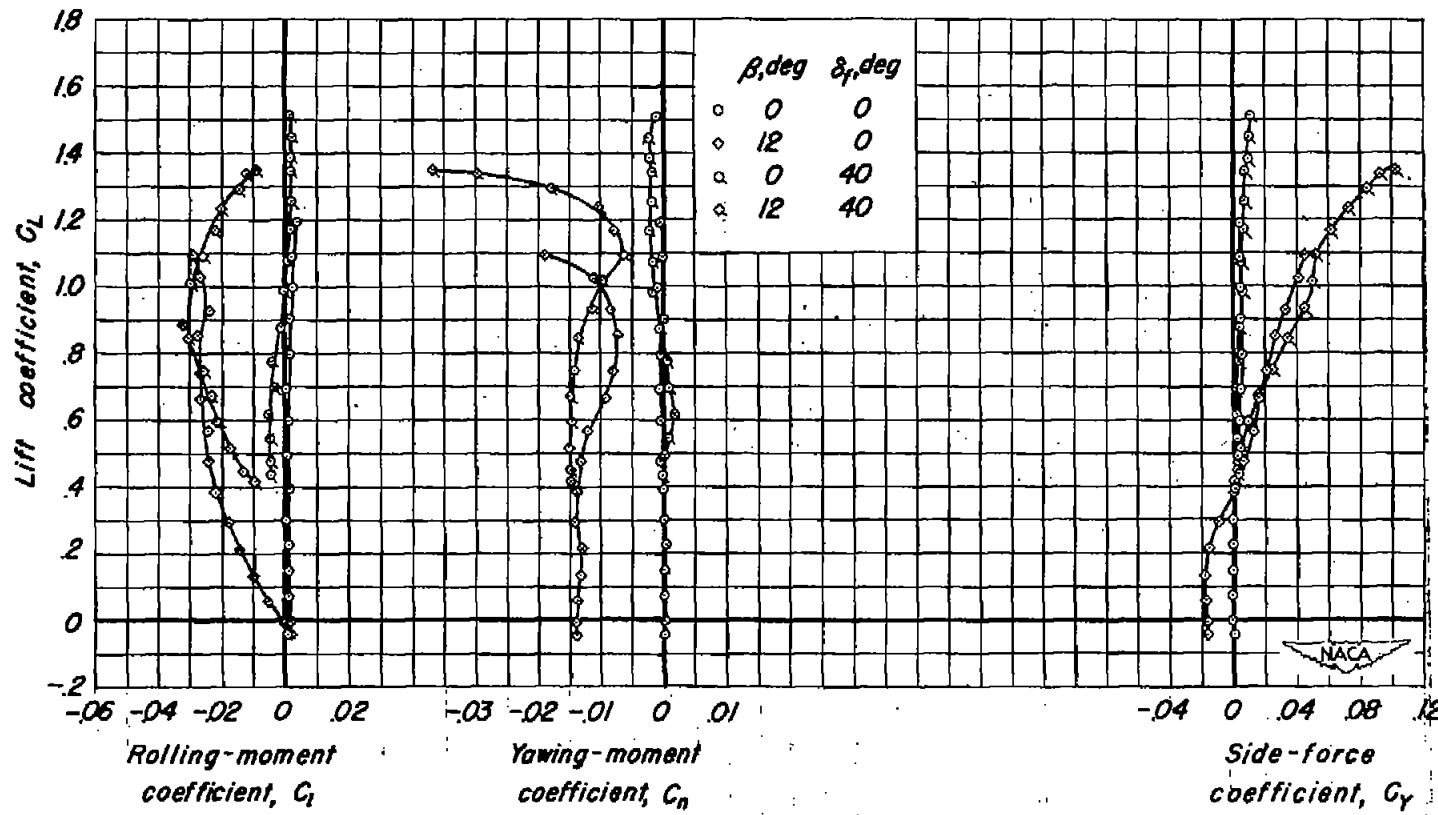
(b)  $C_L$  vs  $C_I$ ,  $C_n$ ,  $C_y$ 

Figure 5.—Concluded.

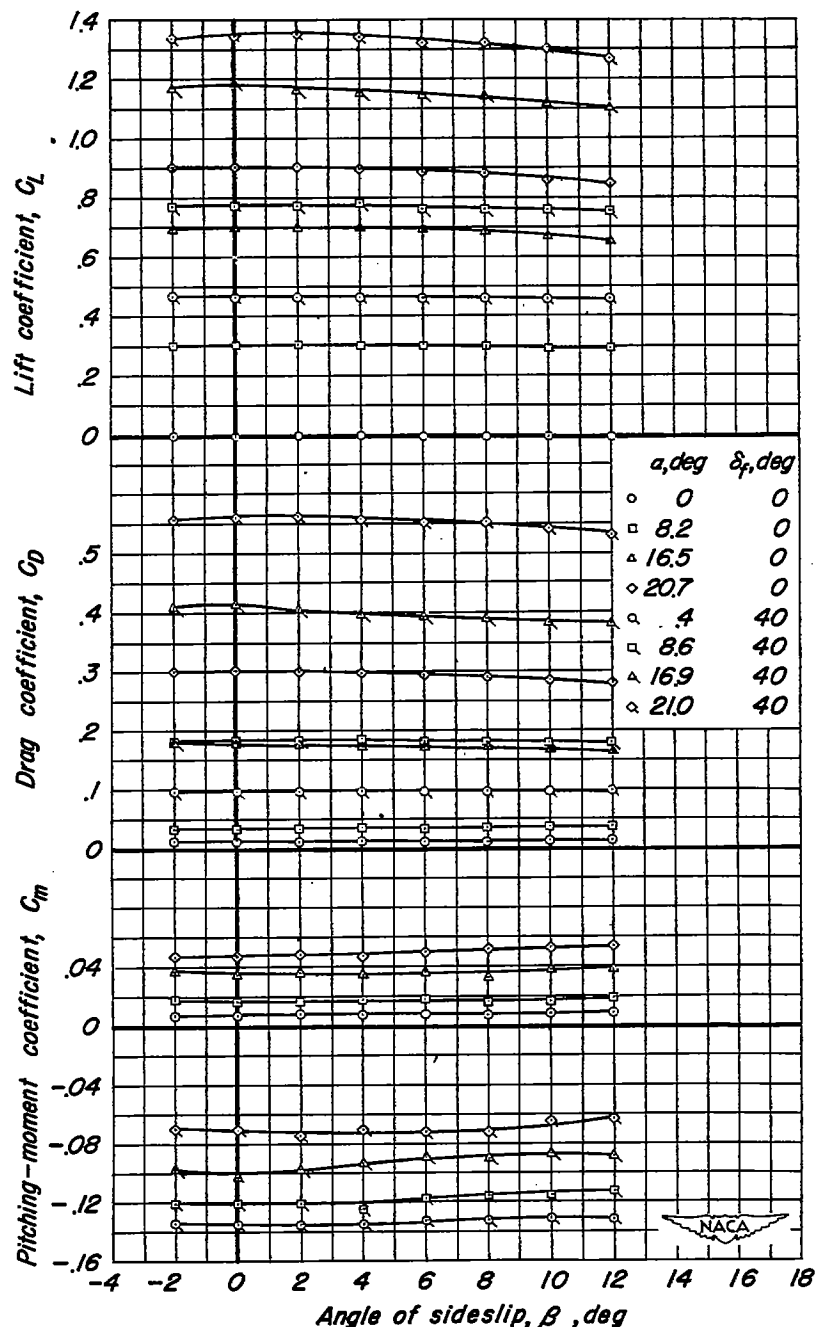
(a)  $C_L$ ,  $C_D$ ,  $C_m$  vs  $\beta$ 

Figure 6.—Characteristics in sideslip of the wing-fuselage combination.

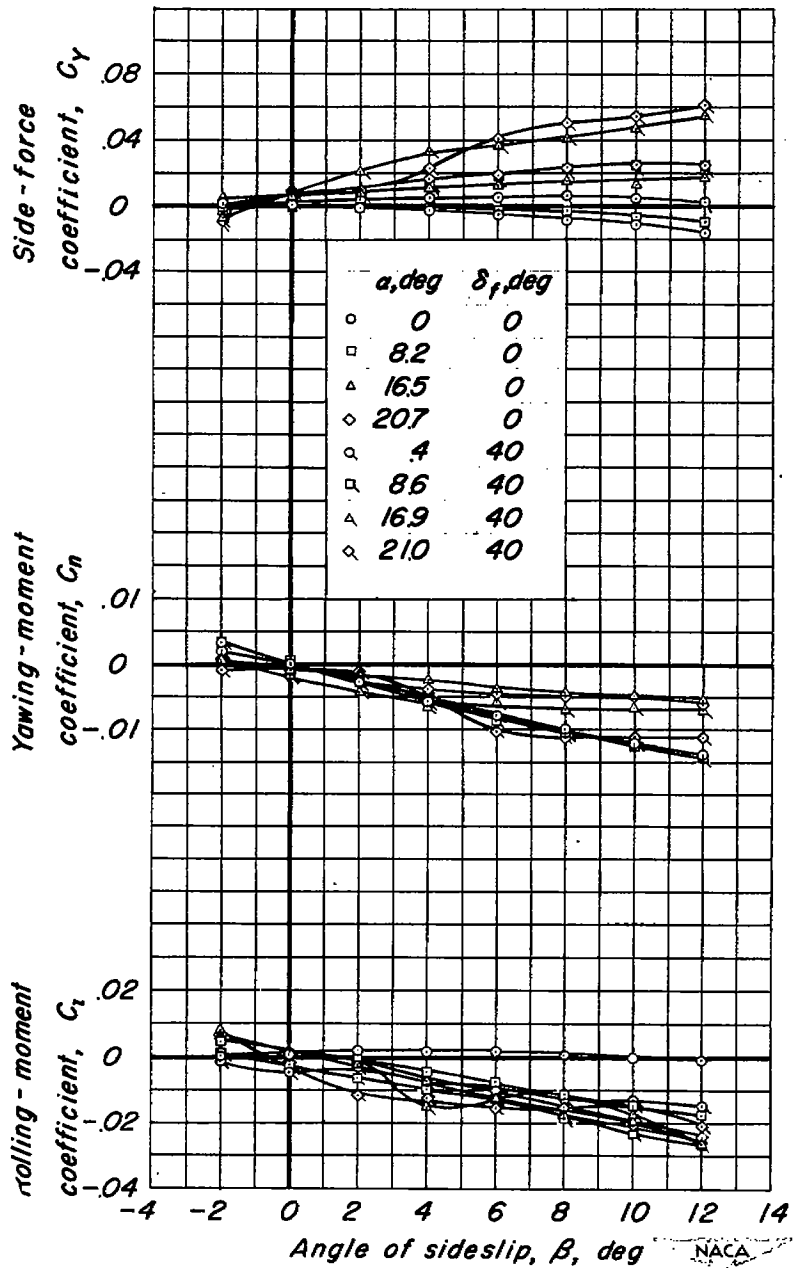
~~CONFIDENTIAL~~(b)  $C_y$ ,  $C_n$ ,  $C_r$  vs  $\beta$ 

Figure 6.— Concluded.

~~CONFIDENTIAL~~

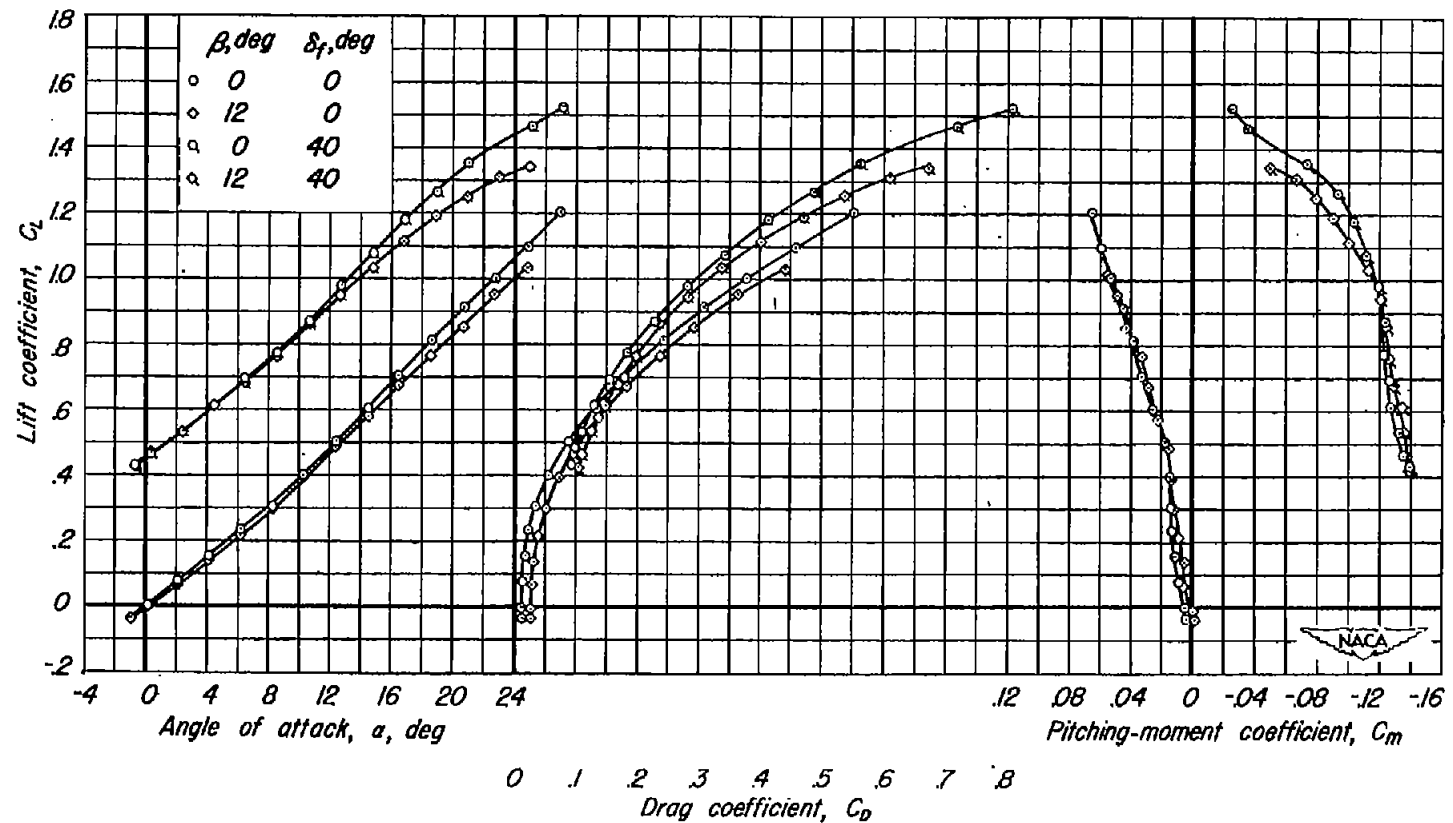
(a)  $C_L$  vs  $\alpha$ ,  $C_D$ ,  $C_m$ 

Figure 7.— Characteristics of the wing-fuselage — vertical-tail configuration at two angles of sideslip and with two trailing-edge flap deflections.

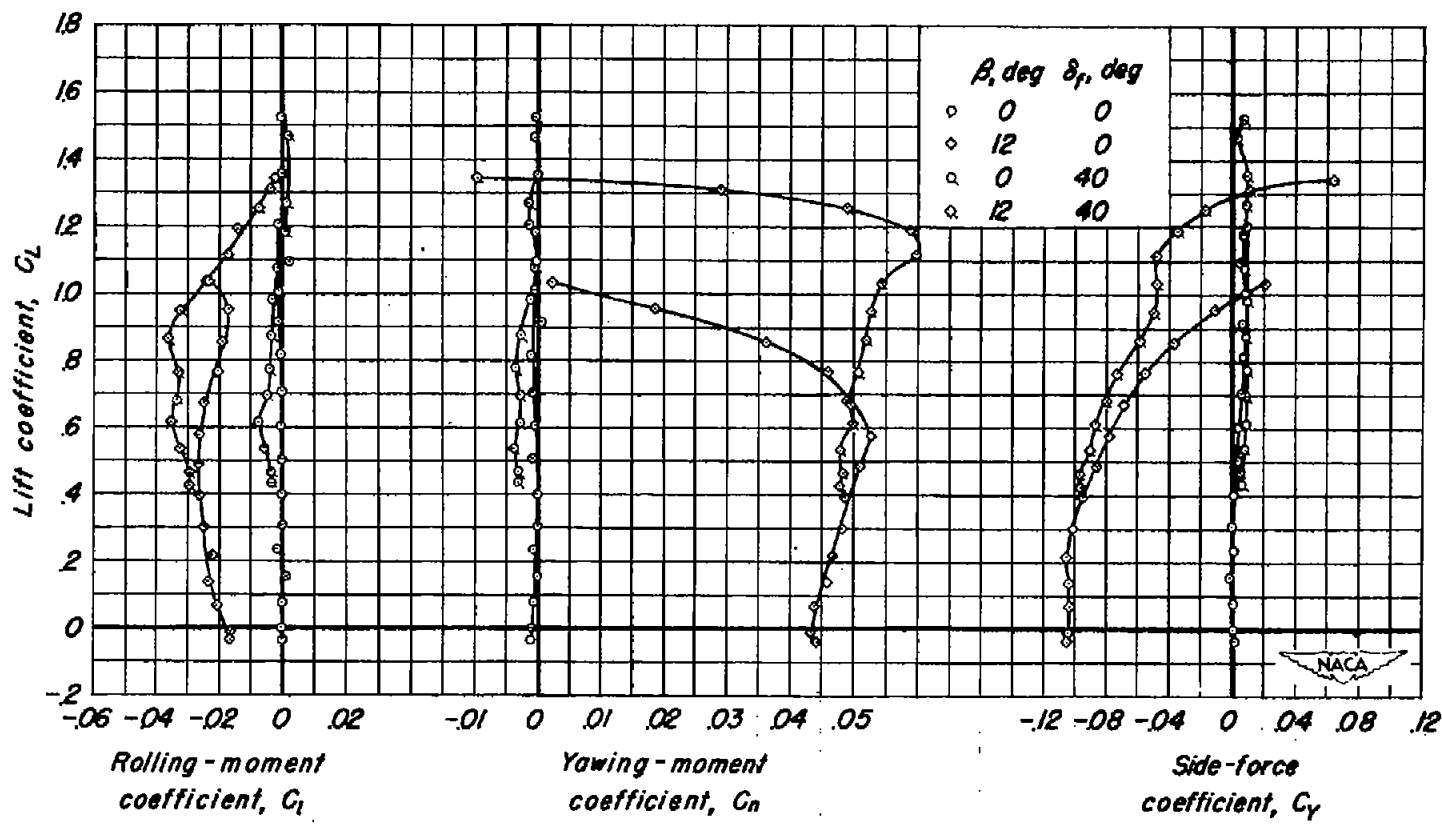
(b)  $C_L$  vs  $C_I$ ,  $C_n$ ,  $C_y$ 

Figure 7.—Concluded.

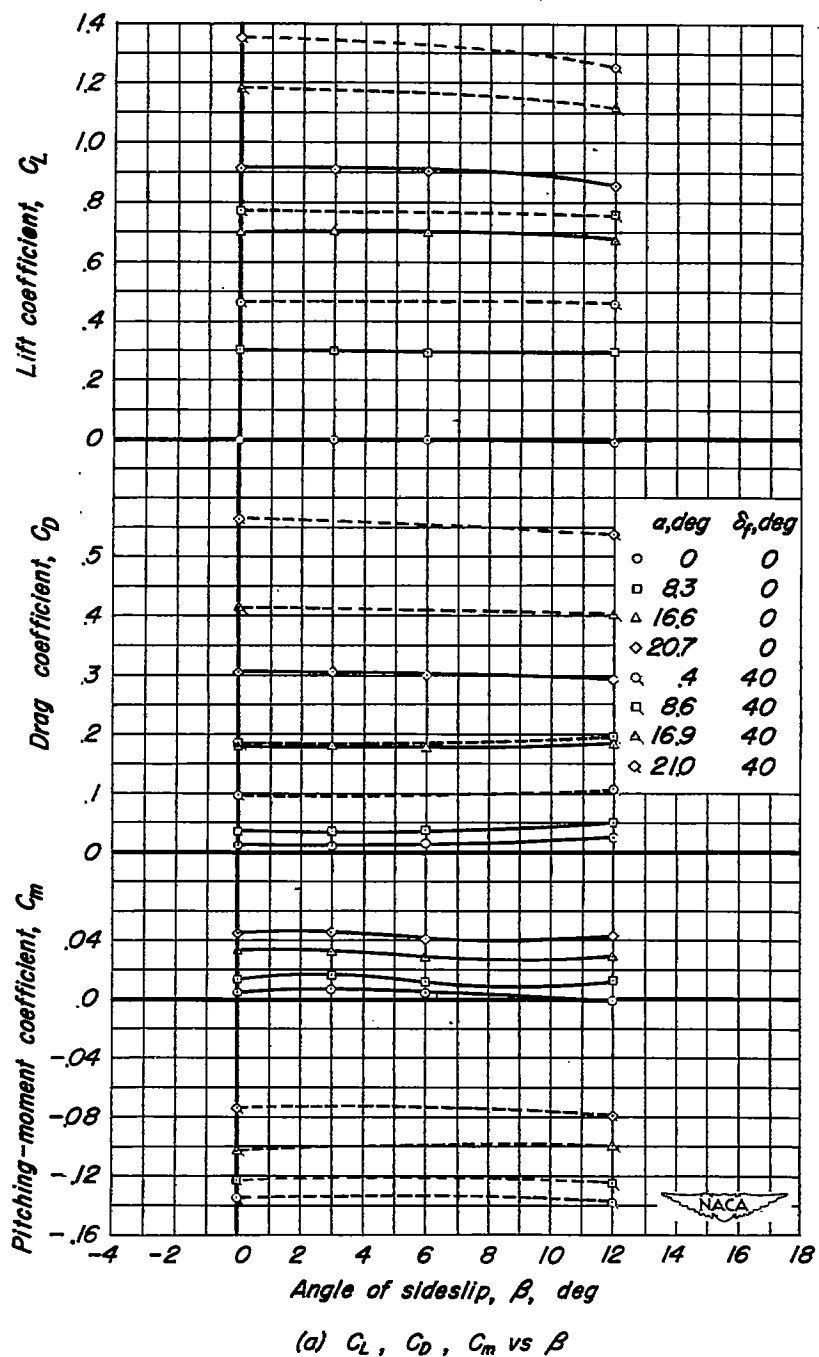
(a)  $C_L$ ,  $C_D$ ,  $C_m$  vs  $\beta$ 

Figure 8.— Characteristics in sideslip of the wing-fuselage - vertical-tail configuration.

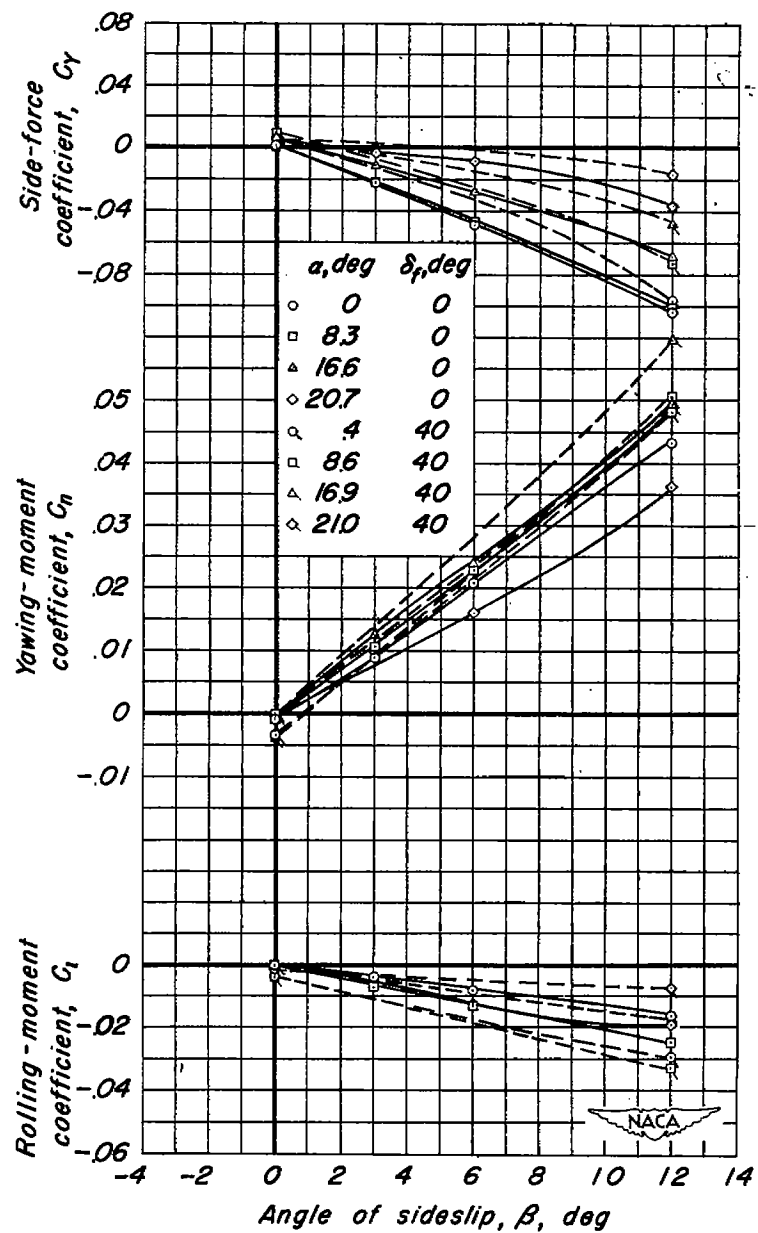
(b)  $C_y$ ,  $C_n$ ,  $C_l$  vs  $\beta$ 

Figure 8.—Concluded.

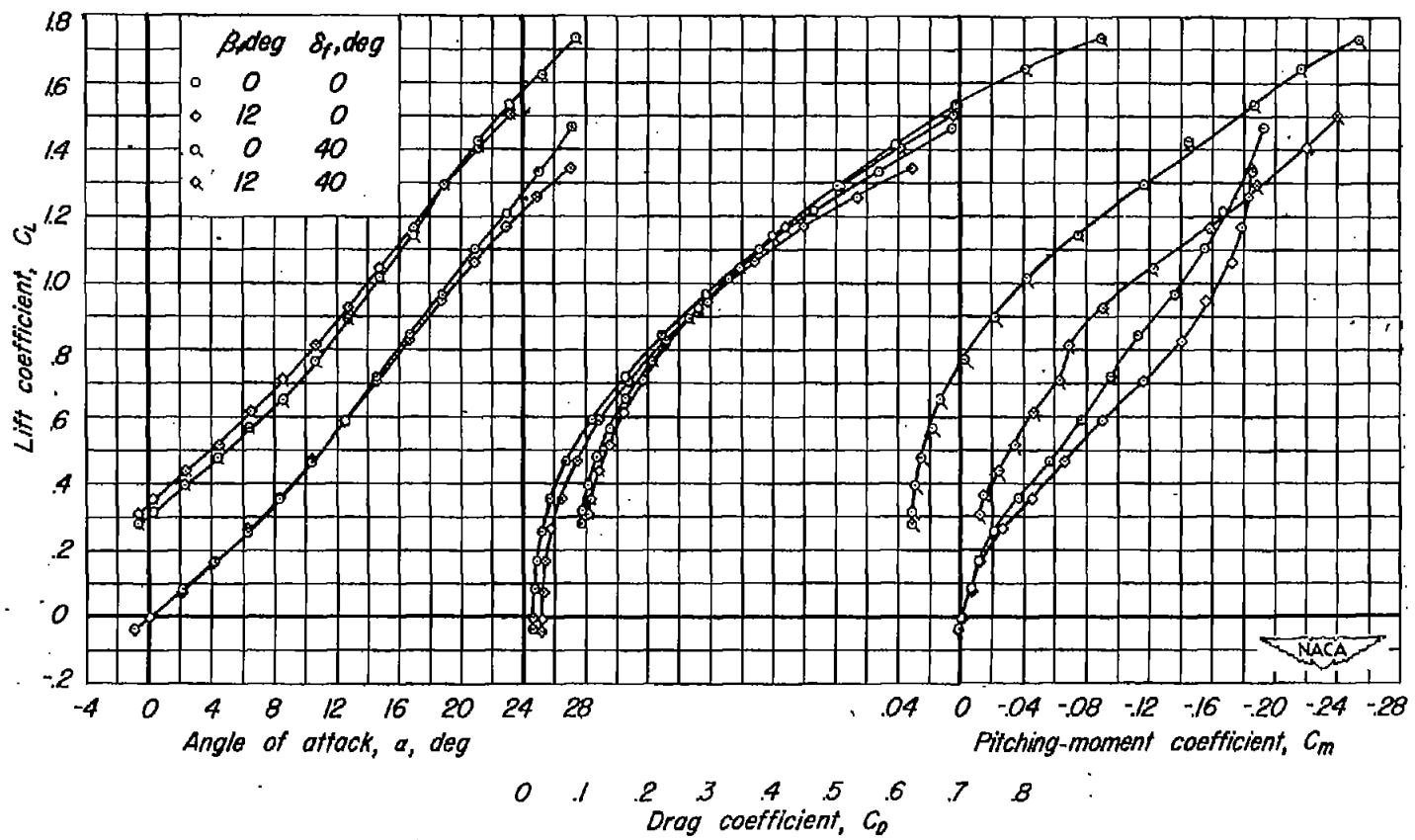
(a)  $C_L$  vs  $\alpha$ ,  $C_D$ ,  $C_m$ 

Figure 9.—Characteristics of the complete model at two angles of sideslip and with two trailing-edge flap deflections.  $i_t = 0^\circ$ .

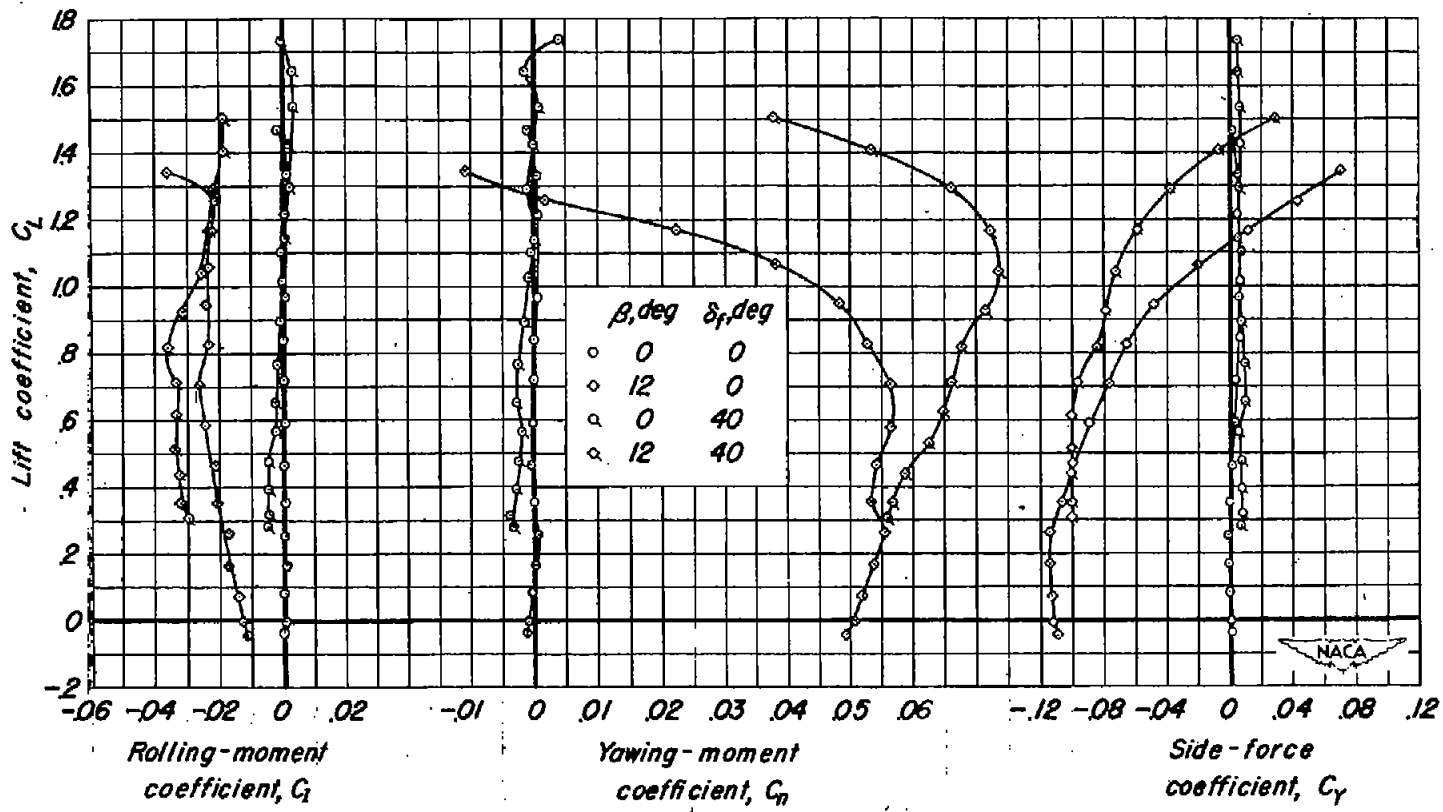
(b)  $C_L$  vs  $C_I$ ,  $C_n$ ,  $C_r$ 

Figure 9.—Concluded.

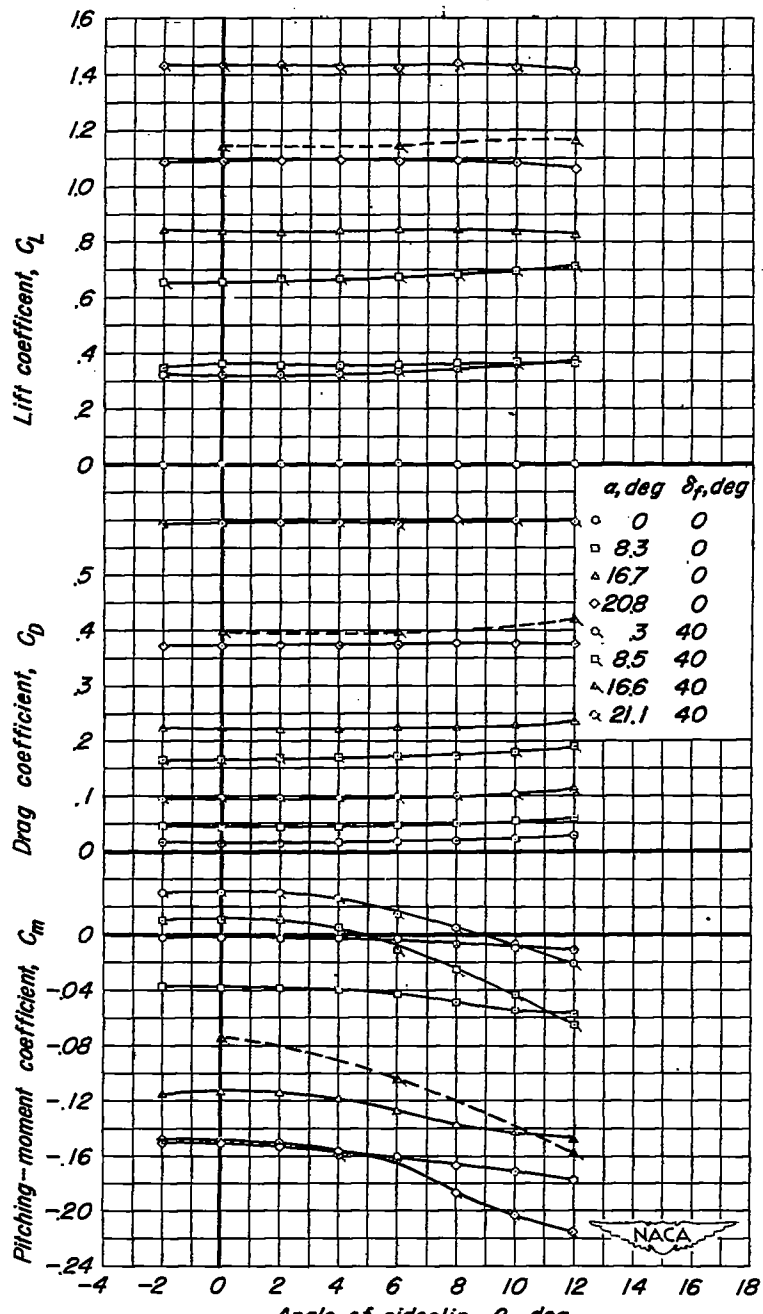
(a)  $C_L$ ,  $C_D$ ,  $C_m$  vs  $\beta$ 

Figure 10.—Characteristics in sideslip of the complete model.  $i_t$ , 0°.

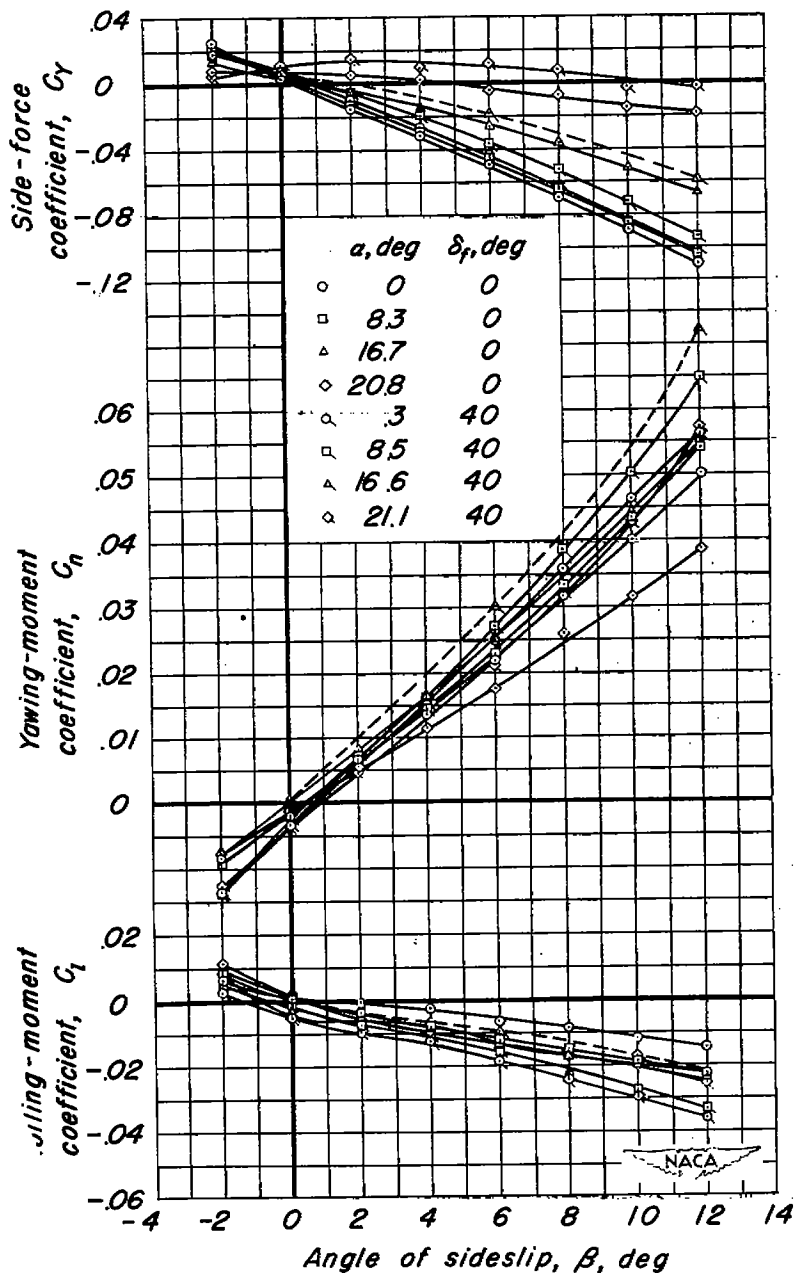
(b)  $C_y$ ,  $C_n$ ,  $C_l$  vs  $\beta$ 

Figure 10.—Concluded.

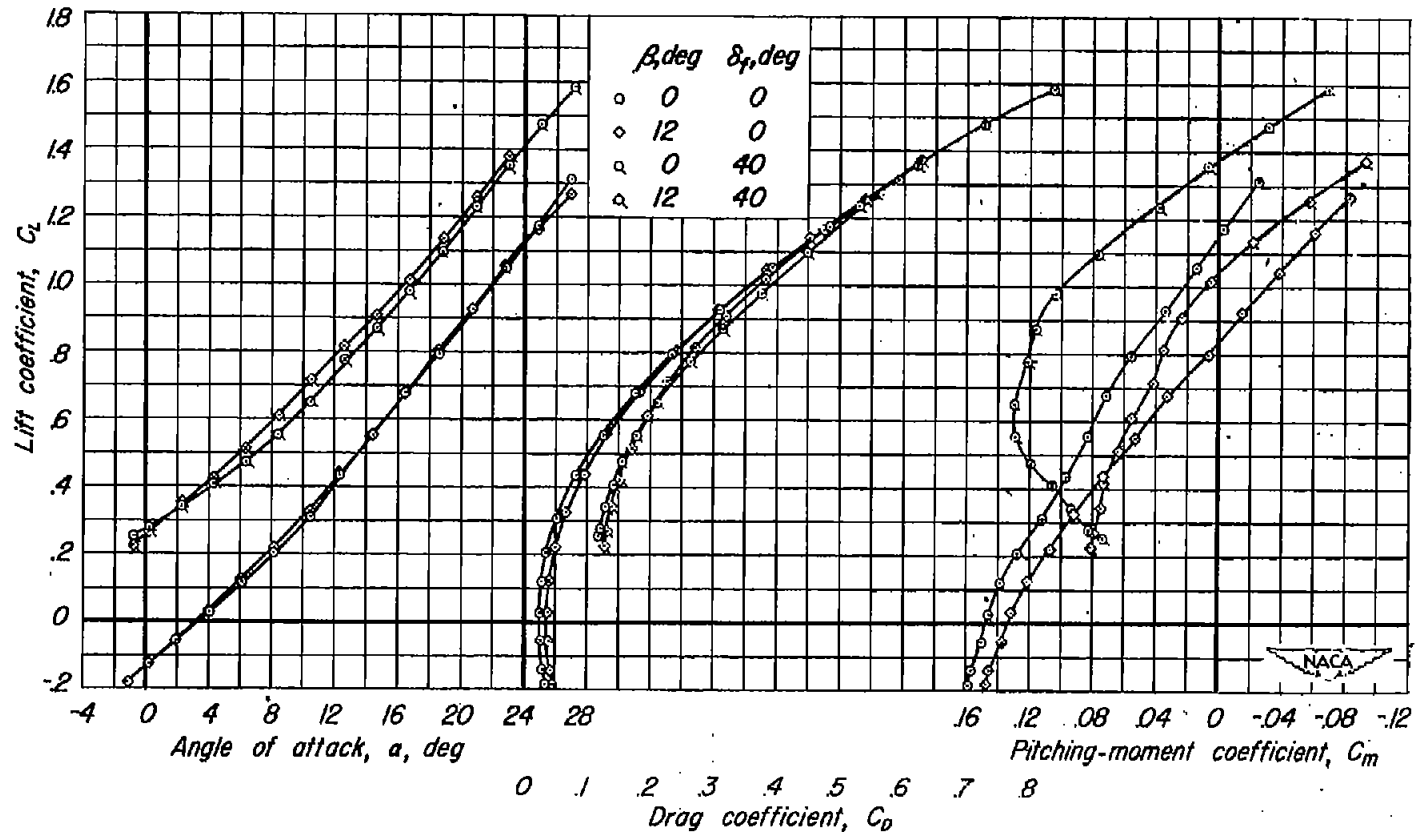
(a)  $C_L$  vs  $\alpha$ ,  $C_D$ ,  $C_m$ 

Figure II.—Characteristics of the complete model at two angles of sideslip and with two trailing-edge flap deflections.  $i_t = -10^\circ$ .

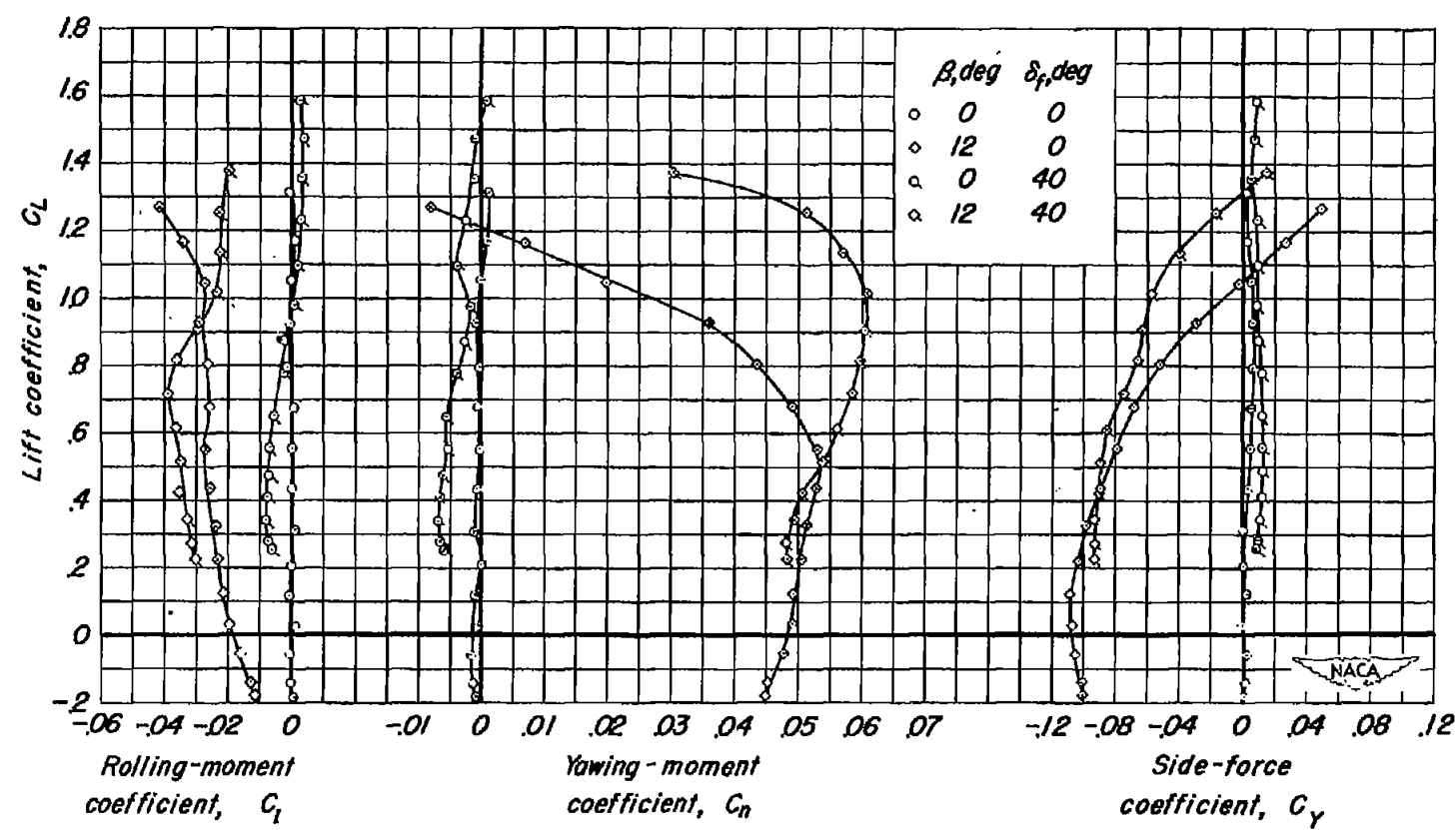
(b)  $C_L$  vs  $C_I$ ,  $C_n$ ,  $C_Y$ 

Figure 11.—Concluded.

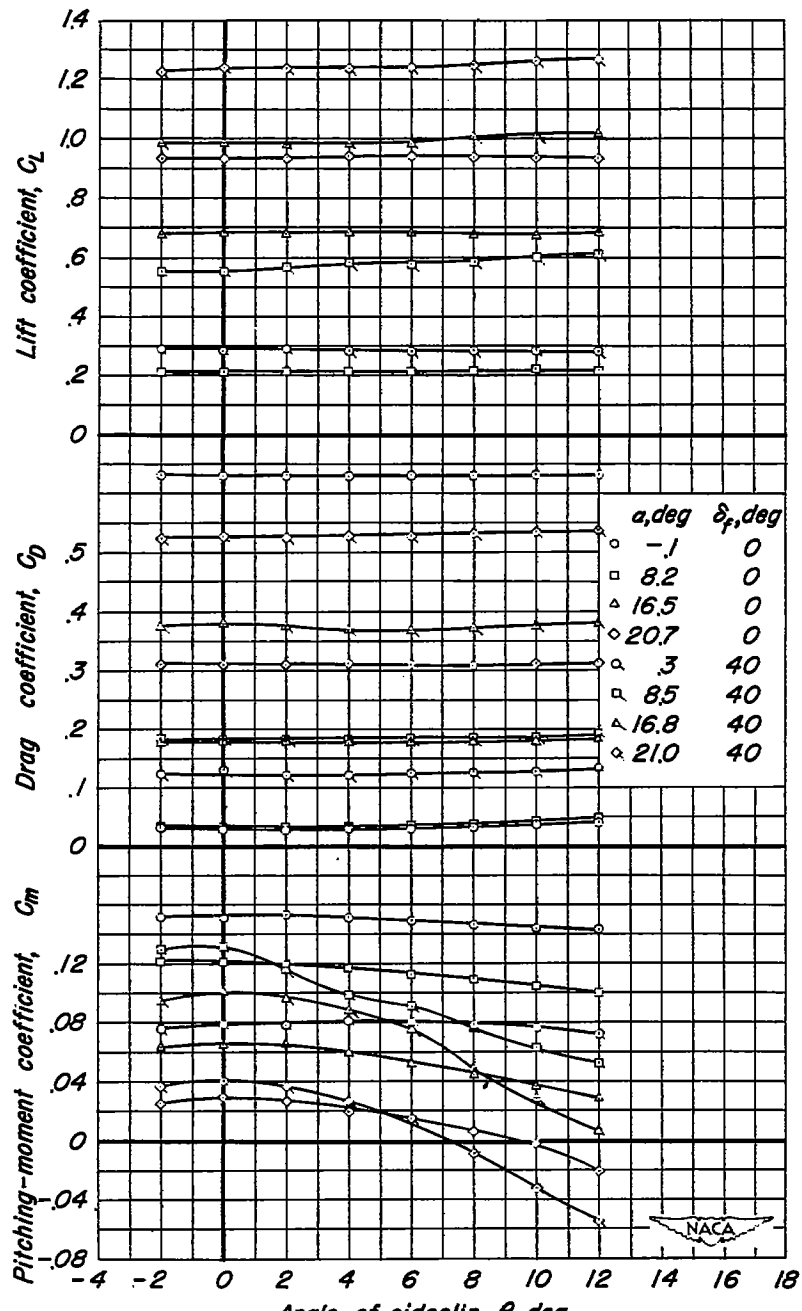
(a)  $C_L$ ,  $C_D$ ,  $C_m$  vs  $\beta$ 

Figure 12.— Characteristics in sideslip of the complete model.  $i_t = -10^\circ$ .

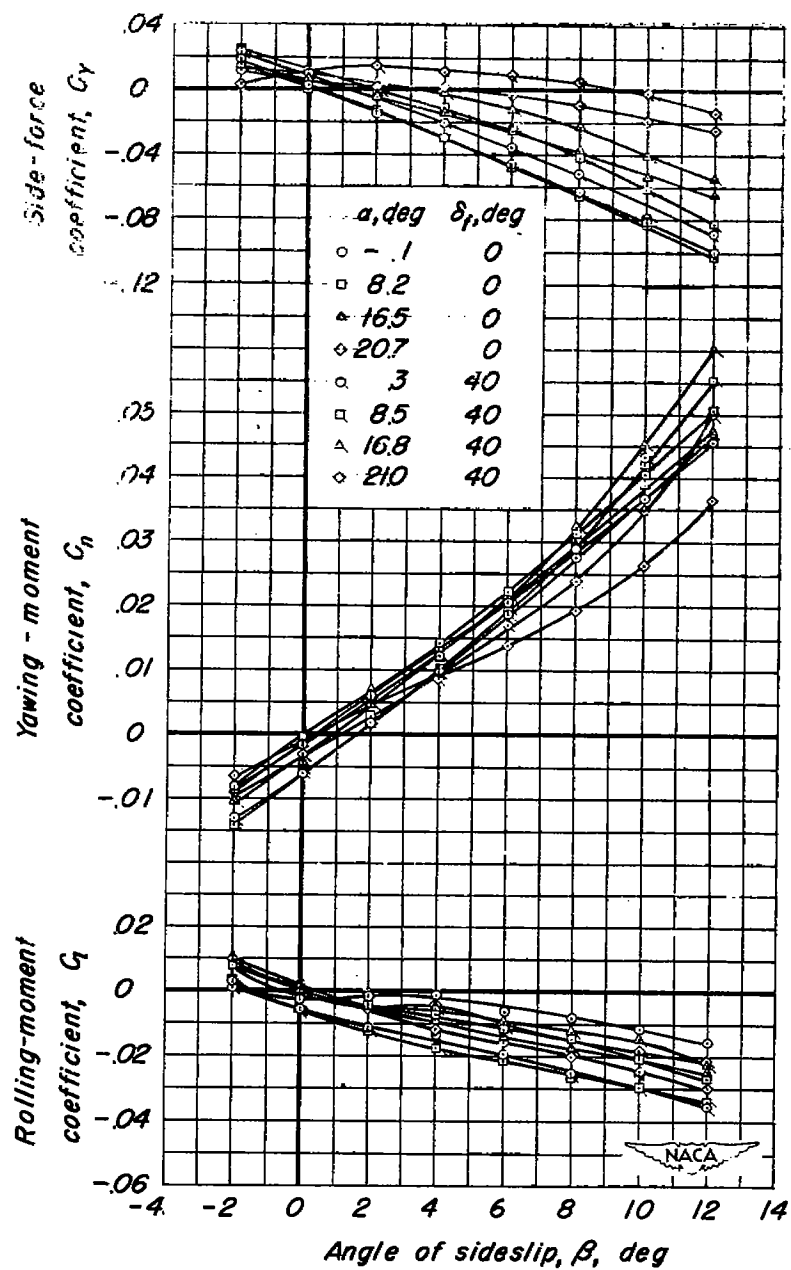
(b)  $C_y$ ,  $C_n$ ,  $C_l$  vs  $\beta$ 

Figure 12.— Concluded.

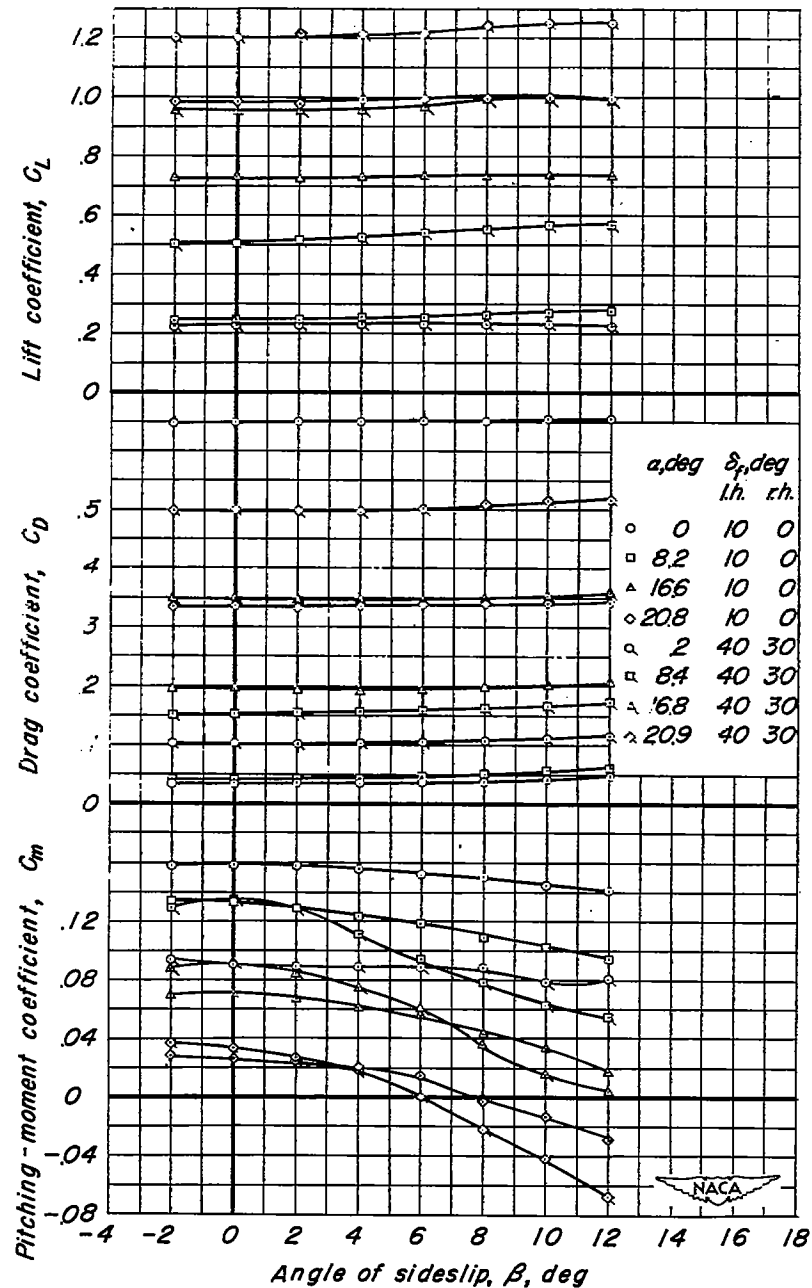
(a)  $C_L$ ,  $C_D$ ,  $C_m$  vs  $\beta$ 

Figure 13.—Effectiveness of trailing-edge flaps used as lateral-control devices.  
 $i_t = -10^\circ$ .

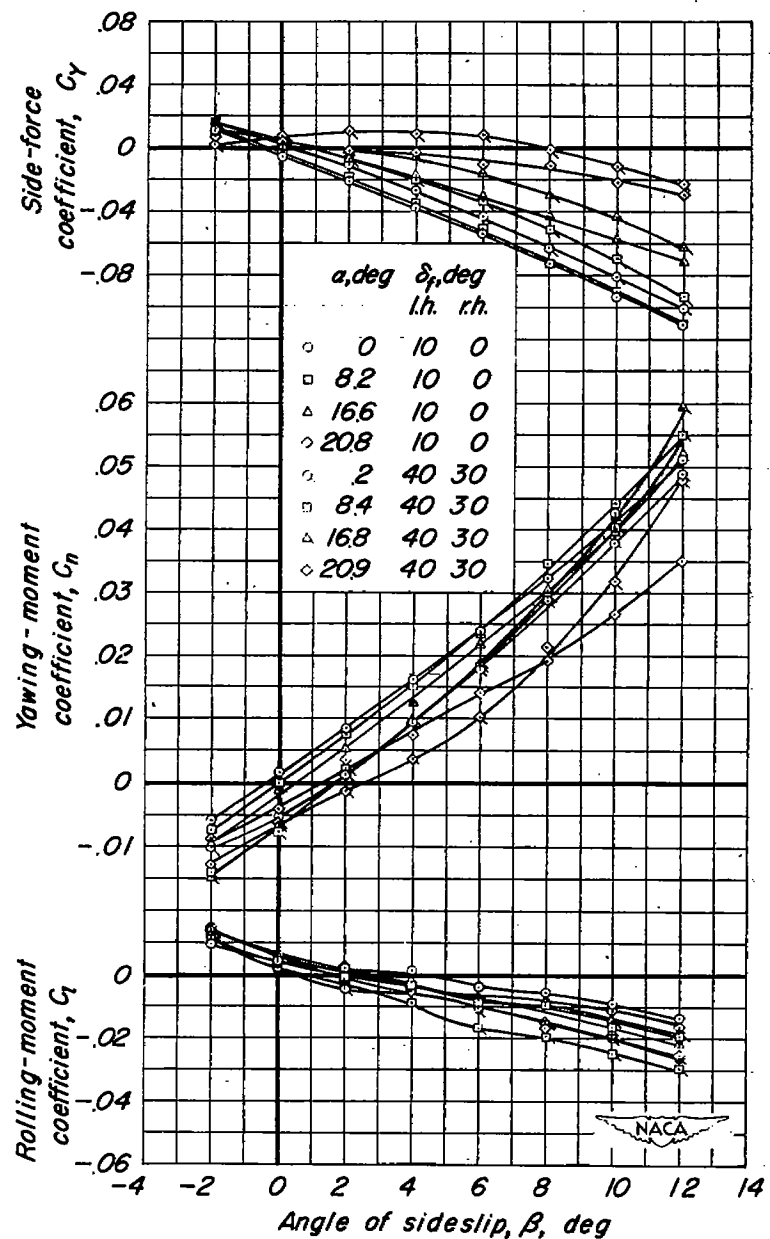
(b)  $C_y$ ,  $C_n$ ,  $C_l$  vs  $\beta$ 

Figure 13.—Concluded.

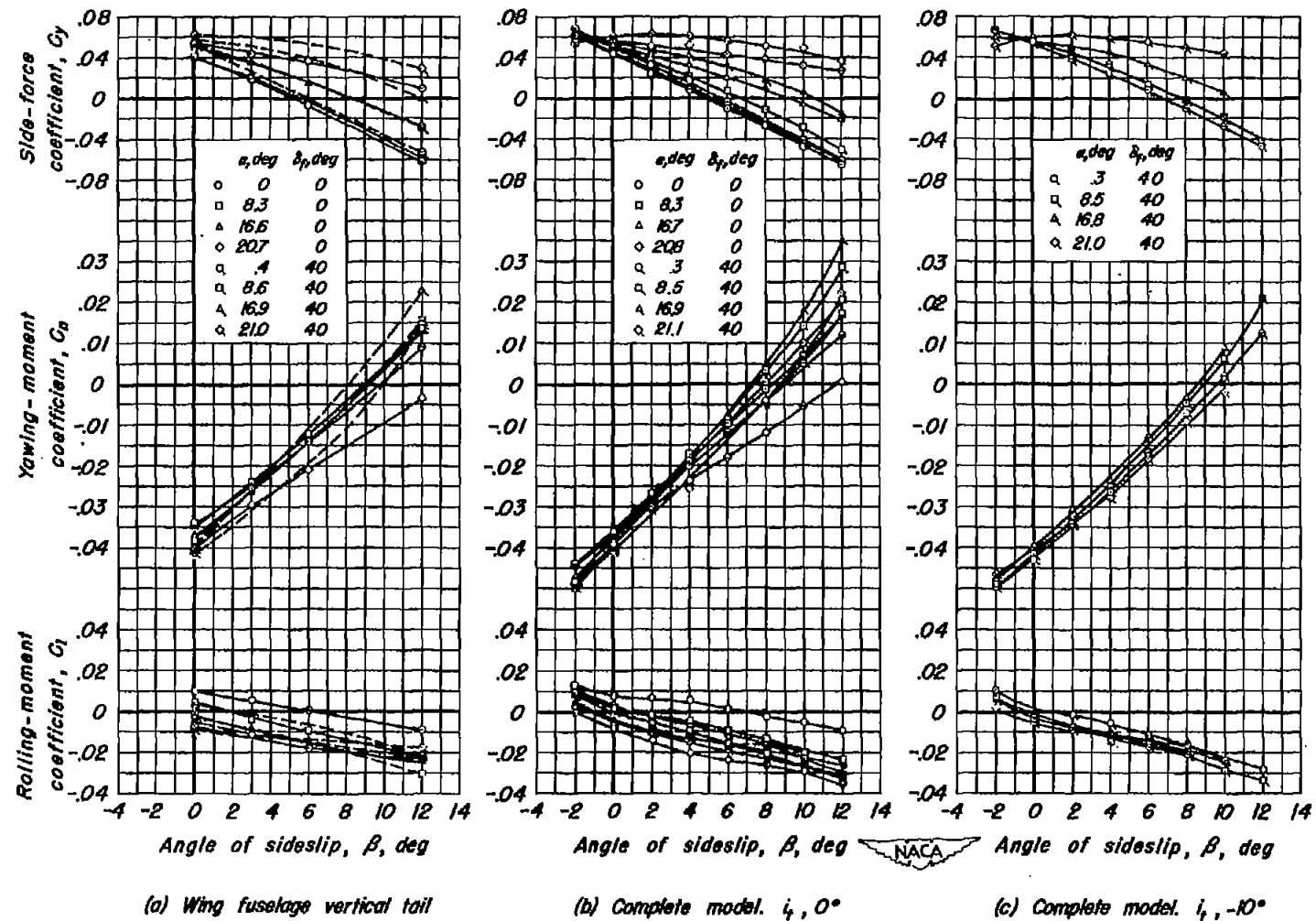


Figure 14.—Effect of the addition of the horizontal tail on the directional control effectiveness.  $\delta_r, 10^\circ$ .

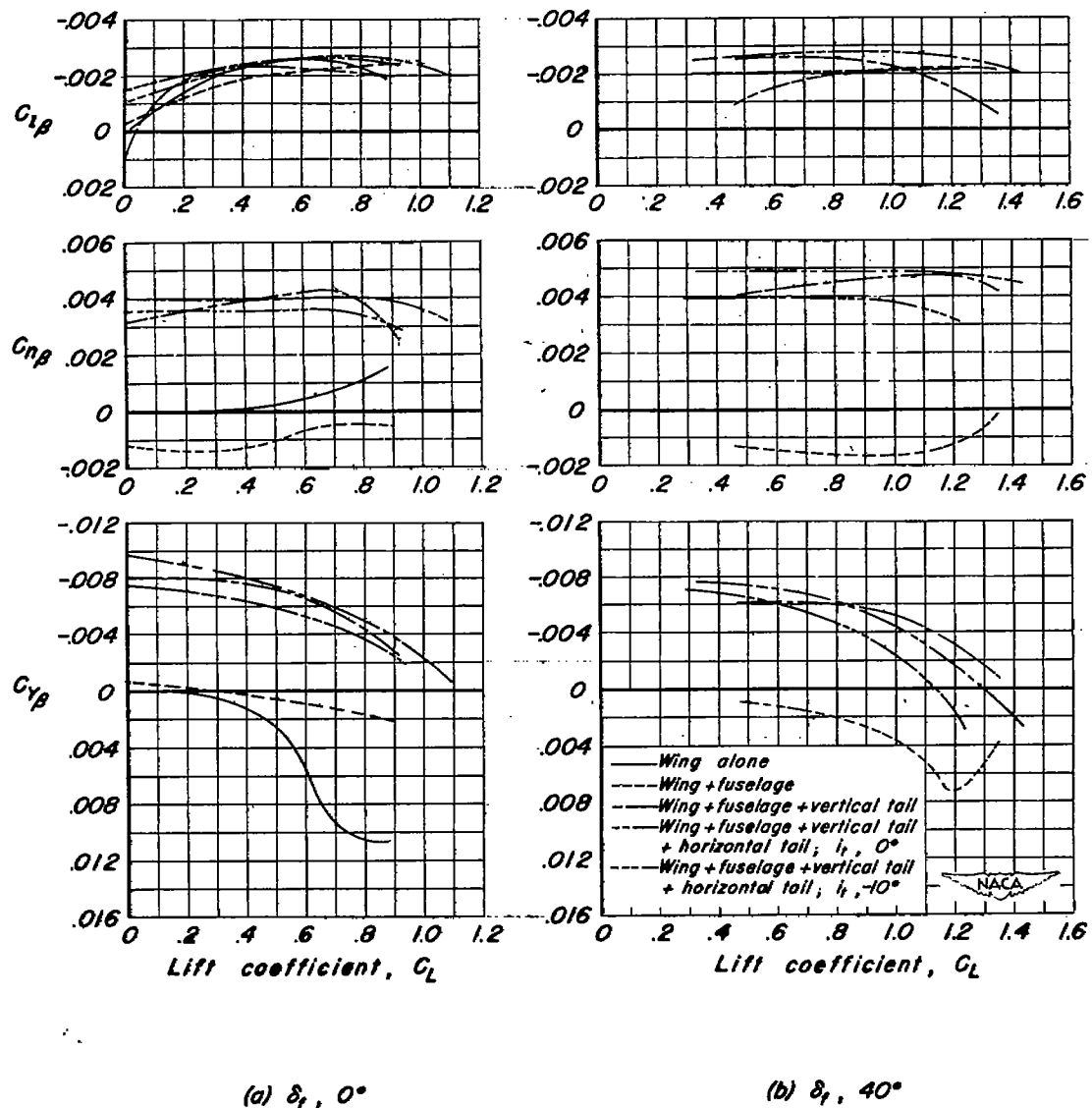


Figure 15.— Stability derivatives of the various configurations.  $\delta_e, 0^\circ$ ;  $\delta_r, 0^\circ$ .

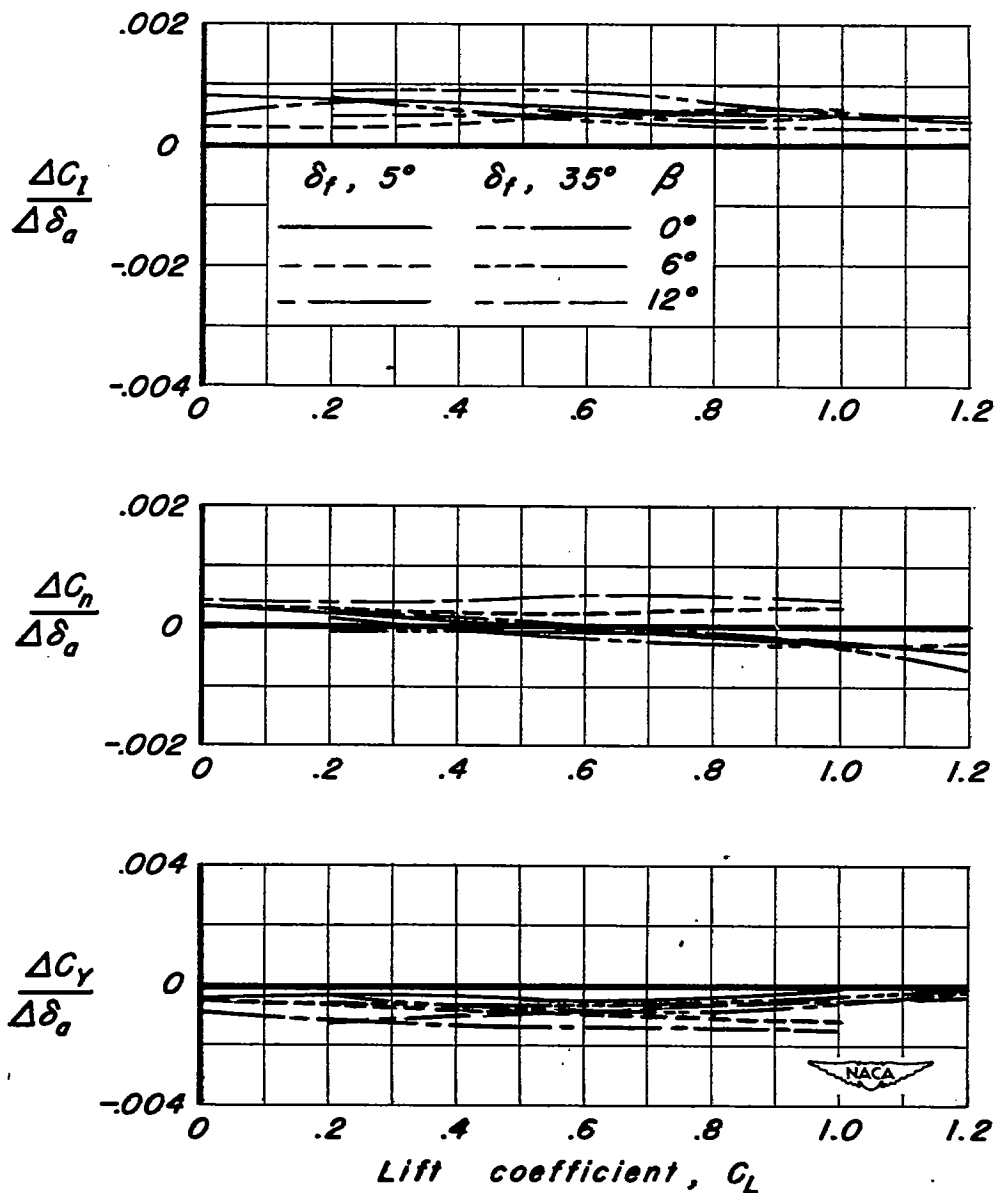


Figure 16.—Increment of rolling-moment, yawing-moment, and side-force coefficients per degree of total aileron deflection, as superposed on  $5^\circ$  and  $35^\circ$  flap deflections.  $\Delta\delta_a$ ,  $10^\circ$ ;  $i_t$ ,  $-10^\circ$ ;  $\delta_r$ ,  $0^\circ$ .

~~CONFIDENTIAL~~

NACA RM A51L03

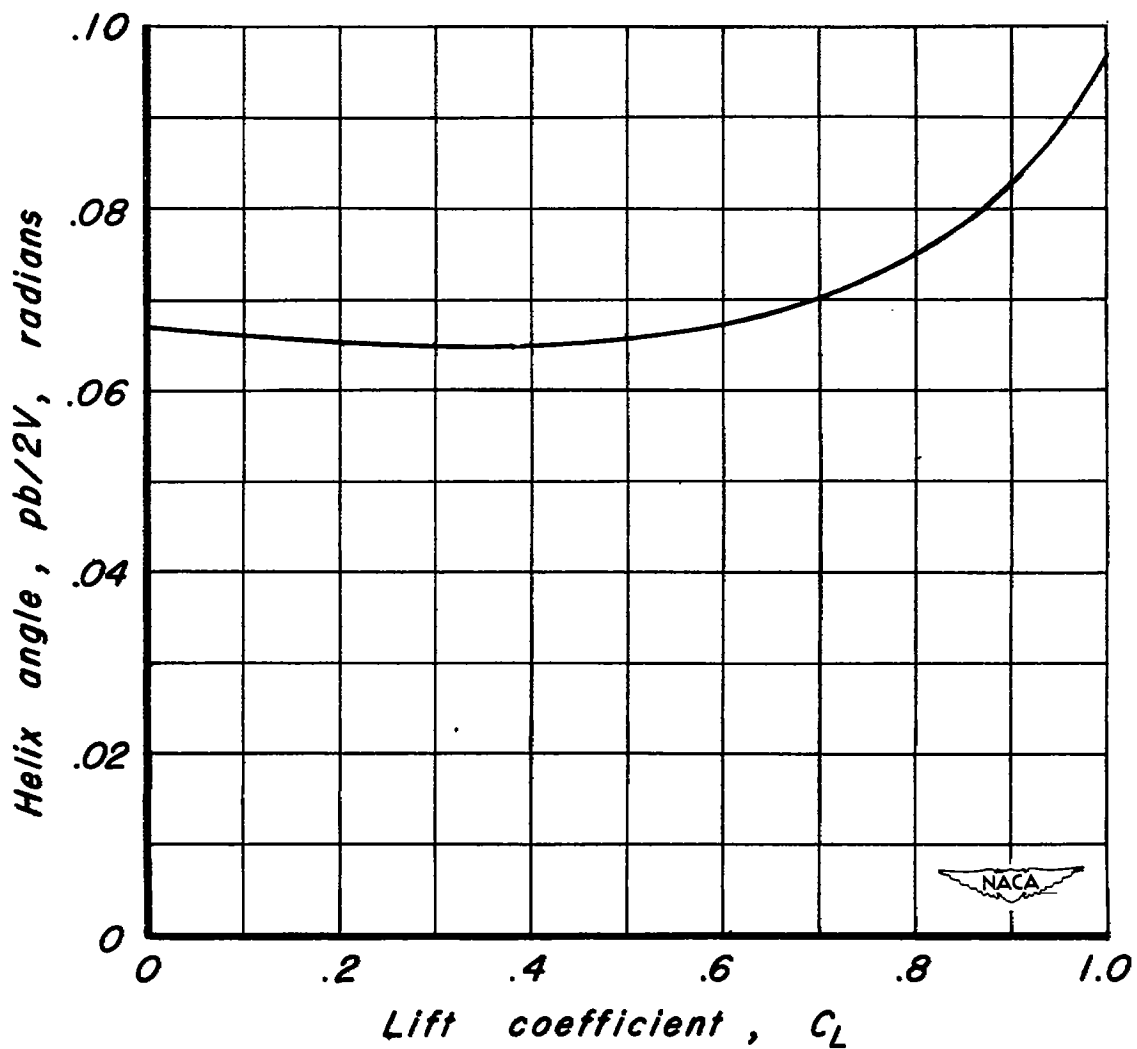
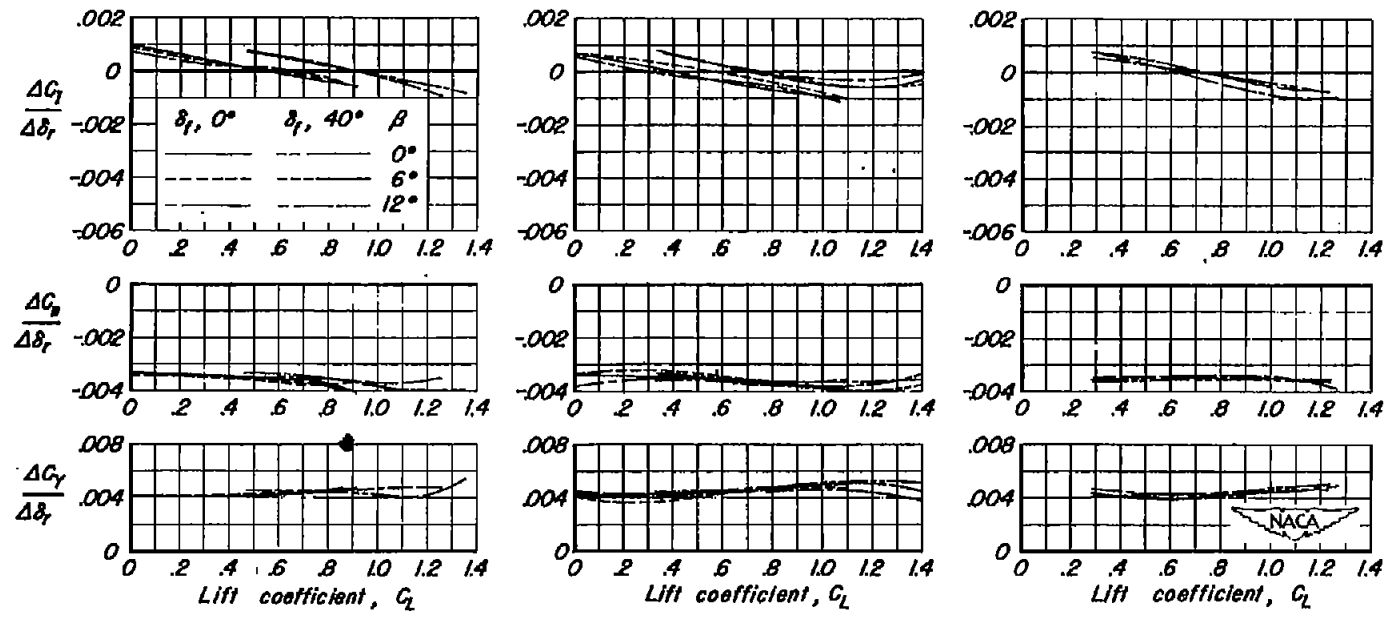


Figure 17.—Variation of wing-tip helix angle with lift coefficient for 10° total aileron deflection.  $\delta_f$ , 5°;  $i_t$ , -10°;  $\delta_r$ , 0°.

~~CONFIDENTIAL~~



(a) Wing fuselage vertical tail

(b) Complete model.  $i_t, 0^\circ$ (c) Complete model.  $i_t, -10^\circ$ 

Figure 18.—Effect of the addition of the horizontal tail on the increments of rolling-moment, yawing-moment and side-force coefficients per degree of rudder deflection.  $\Delta\delta_r, 10^\circ$ ;  $\delta_a, 0^\circ$ .

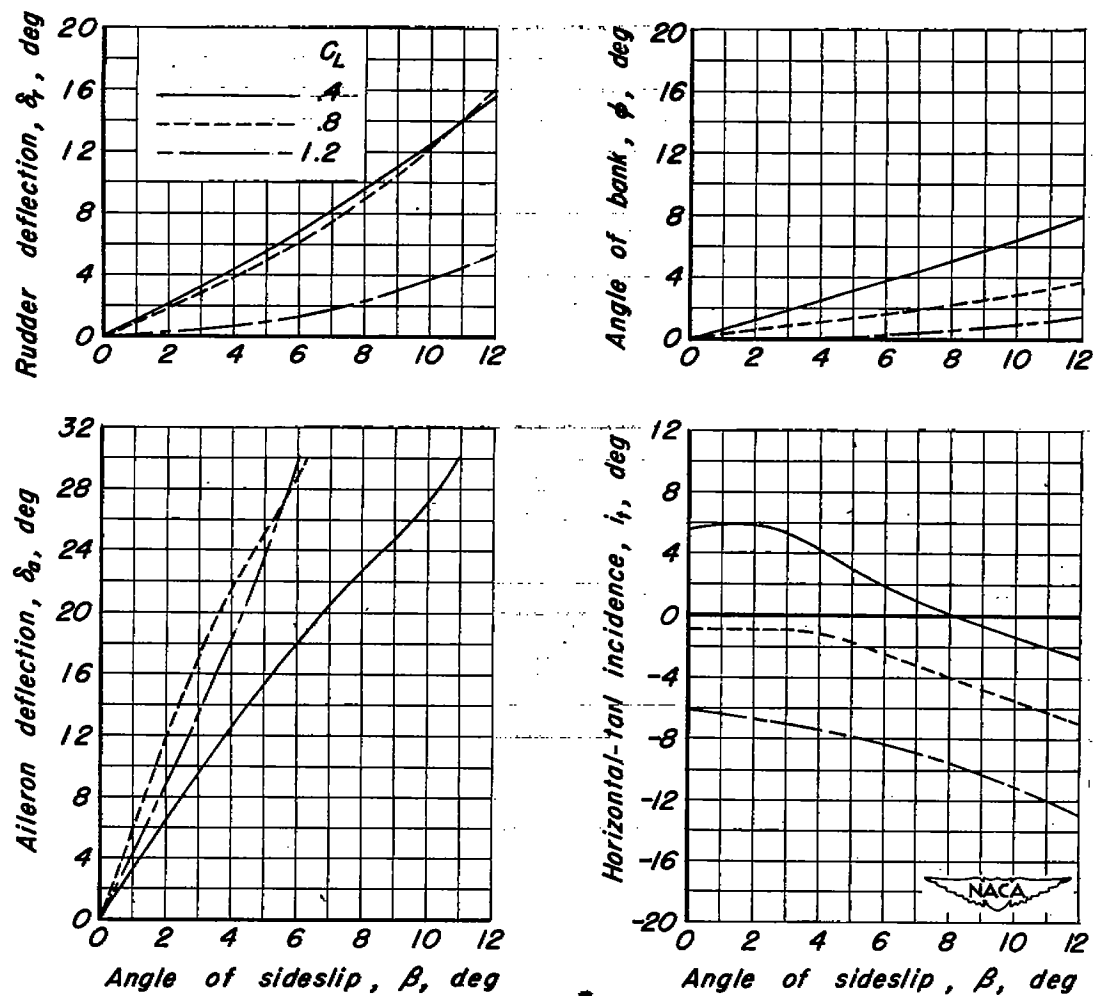


Figure 19.— Control deflections and angle of bank necessary to hold steady sideslip at three given lift coefficients.  $\delta_f$ ,  $40^\circ$ .

**SECURITY INFORMATION**



3 1176 01434 8339

[REDACTED]

[REDACTED]